Age systematics of two young en echelon Samoan volcanic trails

Anthony A. P. Koppers

College of Oceanic and Atmospheric Sciences, Oregon State University, 104 COAS Administration Building, Corvallis, Oregon 97331–5503, USA (akoppers@coas.oregonstate.edu)

Institute of Geophysics and Planetary Physics, Scripps Institution of Oceanography, University of California, San Diego, La Jolla, California 92093–0225, USA

Jamie A. Russell

Institute of Geophysics and Planetary Physics, Scripps Institution of Oceanography, University of California, San Diego, La Jolla, California 92093–0225, USA

Jed Roberts

Department of Geosciences, Oregon State University, Corvallis, Oregon 97331–5506, USA

Oregon Department of Geology and Mineral Industries, 800 NE Oregon Street, Suite 965, Portland, Oregon 97232–2162, USA

Matthew G. Jackson

Department of Geology and Geophysics, Woods Hole Oceanographic Institution, Woods Hole, Massachusetts 02543, USA

Department of Earth Sciences, Boston University, 675 Commonwealth Avenue, Boston, Massachusetts 02215, USA

Jasper G. Konter

Institute of Geophysics and Planetary Physics, Scripps Institution of Oceanography, University of California, San Diego, La Jolla, California 92093–0225, USA

Department of Geological Sciences, University of Texas at El Paso, 500 West University Avenue, El Paso, Texas 79968, USA

Dawn J. Wright

Department of Geosciences, Oregon State University, Corvallis, Oregon 97331–5506, USA

Hubert Staudigel

Institute of Geophysics and Planetary Physics, Scripps Institution of Oceanography, University of California, San Diego, La Jolla, California 92093–0225, USA

Stanley R. Hart

Department of Geology and Geophysics, Woods Hole Oceanographic Institution, Woods Hole, Massachusetts 02543, USA

[1] The volcanic origin of the Samoan archipelago can be explained by one of three models, specifically, by a hot spot forming over a mantle plume, by lithospheric extension resulting from complex subduction tectonics in the region, or by a combination of these two processes, either acting sequentially or synchronously. In this

paper, we present results of 36 high-resolution ^{40}Ar/^{39}Ar incremental heating age analyses for the initial (submarine) phase of Samoan volcanoes, ranging from 13.2 Ma for the westernmost Samoan seamounts to 0.27 Ma in the eastern Samoan volcanic province. Taken as a whole, our new age data point to a hot spot origin for the shield-building volcanism in the Samoan lineament, whereby seamounts younger than 5 Ma are consistent with a model of constant 7.1 cm/yr plate motion, analogous to GPS measurements for the Pacific Plate in this region. This makes our new ^{40}Ar/^{39}Ar ages of the submarine basalts all older compared to recent absolute plate motion (APM) models by Wessel et al. (2008), which are based on the inversion of twelve *independent* seamount trails in the Pacific relative to a fixed reference frame of hot spots and which predict faster plate motions of around 9.3 cm/yr in the vicinity of Samoa. The Samoan ages are also older than APM models by Steinberger et al. (2004) taking into account the motion of hot spots in the Pacific alone or globally. The age systematics become more complicated toward the younger end of the Samoan seamount trail, where its morphology bifurcates into two en echelon subtracks, termed the VAI and MALU trends, as they emanate from two eruptive centers at Vailulu'u and Malumalu seamount, respectively. Spaced ~50 km apart, the VAI and MALU trends have distinct geochemical characters and independent but overlapping linear ^{40}Ar/^{39}Ar age progressions since 1.5 Ma. These phenomena are not unique to Samoa, as they have been observed at the Hawaiian hot spot, and can be attributed to a geochemical zoning in its underlying mantle source or plume. Moreover, the processes allowing for the emergence of two distinct eruptive centers in the Samoan archipelago, the stepped offset of these subtracks, and their slight obliqueness with respect to the overall seamount trail orientation may very well be controlled by local tectonics, stresses, and extension, also causing the rejuvenated volcanism on the main islands of Savai'i, Upolu, and Tutuila since 0.4 Ma.

1. Introduction

[2] The concept of a hot spot typically is invoked to explain the formation of linear age progressive trails of volcanic islands and seamounts, with a tectonic plate moving over the locus of a stationary mantle plume that has been rising from deep in the Earth's mantle over the course of possibly a hundred million years [*Wilson*, 1963; *Morgan*, 1972]. However, the classical Wilson-Morgan hot spot model is often too simplistic to properly explain the natural complexities of intraplate volcanism and geodynamics, impelling scientists to consider different types of hot spots [*Courtillot et al.*, 2003], the motion of mantle plumes [*Steinberger and O'Connell*, 1998; *Steinberger*, 2000; *Koppers et al.*, 2001; *Tarduno et al.*, 2003, 2009], more dynamic plume behaviors [*Lowman et al.*, 2004; *Lin and van Keken*, 2006; *Davies and Davies*, 2009], and hybrid mod-

els including plate extension as a secondary process [*Koppers and Staudigel*, 2005].

[3] Understanding these complexities of intraplate volcanism requires a better knowledge of the morphology, age and geochemistry of seamount trails at various scales. Assuming that hot spots are formed above mantle plumes with nominal diameters of 200 to 400 km [*Campbell and Griffiths*, 1990; *Montelli et al.*, 2004], it is likely that processes occurring at smaller scales cause noticeable deviations from the linear morphology of seamount trails, disturbances in the age/distance systematics along these trails, and variations in geochemical signatures within a single seamount or between seamounts. These small-scale processes may be explained by the structure of a mantle plume itself, the structure and thickness of the oceanic lithosphere, the preloading and preconditioning of oceanic crust and its underlying asthenosphere by previously formed seamounts

and seamount trails, changes in plate motion, variable magmatic processes, the influence of a nearby spreading center or another plate tectonic boundary, and so on.

[4] Samoa is an excellent example of a complex seamount trail that requires a hybrid model with two distinct stages of intraplate volcanism: (1) an early hot spot/plume stage, which constructed the volcanic shield of Savai'i Island for instance, around 5.0 Ma and (2) a later stage, most likely driven by lithospheric deformation, which formed the posterosional volcanic cap on the islands of Savai'i, Upolu and Tutuila, starting much later, around 0.4 Ma [*Natland*, 1980; *Natland and Turner*, 1985; *Koppers et al.*, 2008]. In addition, toward the young end of the Samoan seamount trail, its morphological expression changes from a robust singular trail into two en echelon trails [*Workman et al.*, 2004], spaced about 50 km apart (Figure 1). This transition happens around 1.5 Ma and each of these subtracks are not longer than 170 km, yet both show evidence for "zero-aged" volcanism at their easternmost ends. In the northern VAI subtrack, volcanism starts at Tamai'i seamount and ends at Vailulu'u, which has been active for at least the last few hundred thousand years, including an (unobserved) eruption happening between 2001 and November 2004 [*Staudigel et al.*, 2006; *Sims et al.*, 2008]. In the southern MALU subtrack, volcanism extends southeastward from the eastern section of Tutuila Island and ends at Malumalu seamount, which has had multiple eruptions within the last 300 Kyr, and one younger than 8 Kyr, based on observed isotopic disequilibrium in ^{230}Th, ^{231}Pa or ^{226}Ra of various dredged samples [*Sims et al.*, 2008].

[5] We will show in this paper that the en echelon subtracks are morphologically separated and have their own geochemical character. We will also show that these subtracks have independent but entirely overlapping linear ^{40}Ar/^{39}Ar age progressions, which are consistent with a constant 7.1 cm/yr plate motion as determined from Global Positioning System (GPS) measurements for the Pacific plate in this region [*Beavan et al.*, 2002; *Sella et al.*, 2002]. These small-scale phenomena are not unique to Samoa and will provide key insights into the geochemical zonation of the underlying mantle plume in this region. Finally, we will discuss what processes might have caused the apparently slower local plate motion as recorded by Samoa's age progression and compared to other seamount trails in the Pacific, the formation of the two subtracks, and the role of local tectonic control (i.e., tectonic stress and extension attributable to the nearby Tonga subduction zone)

that plausibly also may be responsible for the younger than ~0.4 Ma rejuvenated volcanism on the main islands of Savai'i, Upolu and Tutuila.

2. Geological Setting

[6] Samoa is a complex trail of volcanic islands and seamounts located approximately 1,500 km south of the equator on the western side of the Pacific Ocean (Figure 1a). Two western islands, Savai'i and Upolu make up the independent country of Samoa, whereas the eastern islands of American Samoa are unincorporated territories of the United States of America. Throughout this paper the eastern and western islands, as well as the numerous seamounts, will collectively be referred to as Samoa, which we further divide into the "Western Samoan volcanic province" (WESAM) and the "Eastern Samoan volcanic province" (ESAM) based on geographic distribution.

[7] Samoa is located very near to the most northeastern part of the Tonga Trench, where the Pacific Plate is subducting beneath the Indian-Australian Plate (Figure 1a). The northeastern point of this trench is referred to as the NE terminus (NET) at which point the trench bends around, turns to the west, and continues into the Vitiaz Lineament [*Wright et al.*, 2000; *Ruellan et al.*, 2003]. This is a convoluted, stepped transform fault plate boundary [*Govers and Wortel*, 2005] that roughly runs along the southern part of the WESAM. Here interactions of the trench and transform fault may be placing stress on localized portions of the Pacific Plate, a condition that likely has been exaggerated by the ultrafast up to 17 cm/yr roll back of the down going Pacific Plate [*Ruellan et al.*, 2003; *Hart et al.*, 2004; *Natland and Winterer*, 2005; *Koppers et al.*, 2008]. This complex tectonic setting in which the Pacific Plate seems to be bending, flexing and tearing [*Hawkins and Natland*, 1975; *Wright*, 1992; *Hart et al.*, 2004] is unique to the South Pacific ocean.

[8] Presently, the NET is located at ~174°W and ~15°S and only ~150 km south of Savai'i Island and ~300 km from the Vailulu'u hot spot location. However, due to the fast 7.1 cm/yr Pacific Plate motion toward the WNW and the ultrafast rollback of the Pacific Plate along the Tonga Trench toward the east, this tectonic situation was drastically different over the last 15 Myr [*Ruellan et al.*, 2003; *Hart et al.*, 2004]. For example, around 4 Ma, the location of the NET was at least five times further away (~1,500 km) from the predicted location of the Samoa hot spot [*Koppers et al.*, 2008]. This makes
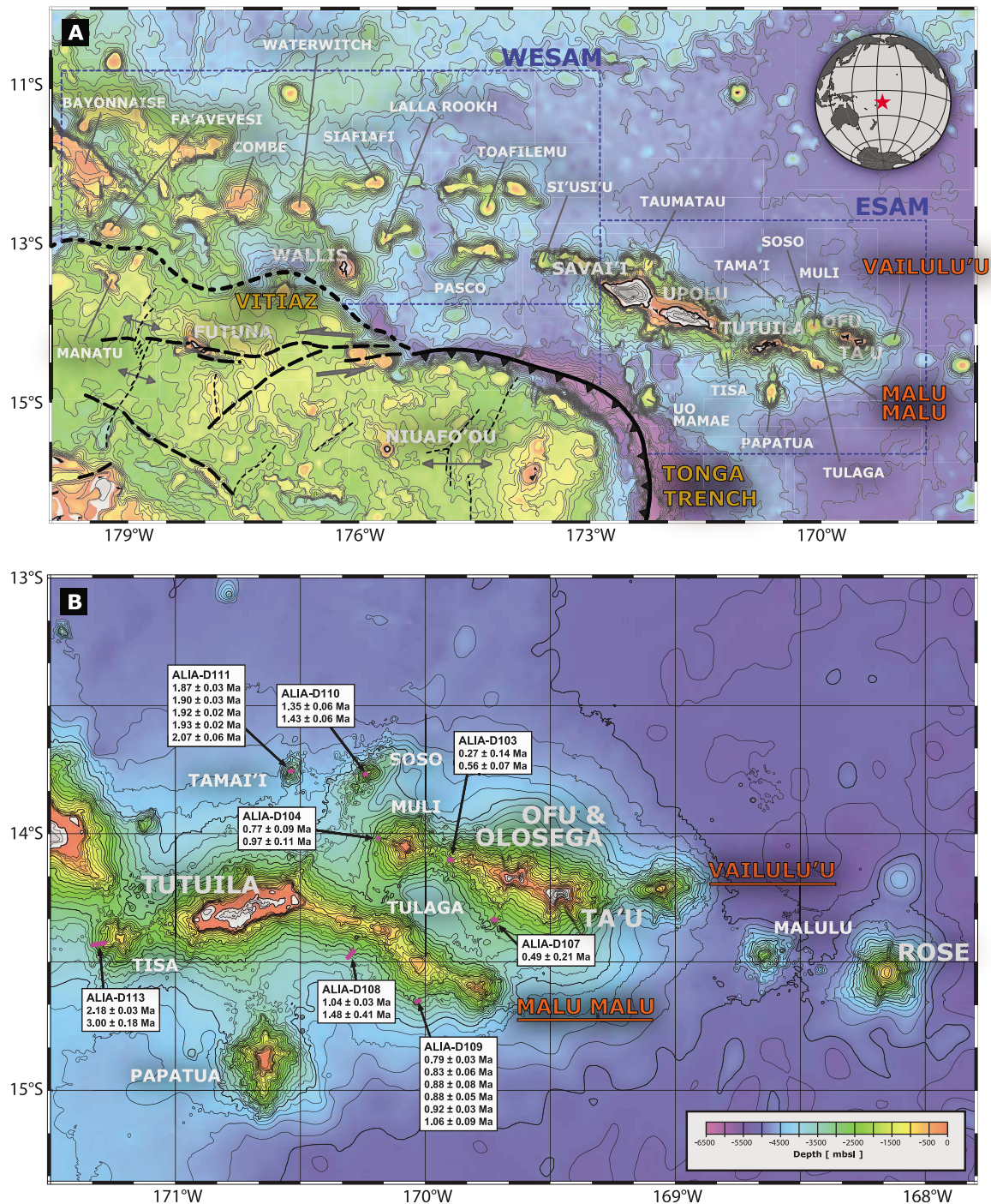
Figure 1. Bathymetric maps of the Samoa seamount trail region based on a combination of SIMRAD EM120 multi-beam data collected during the ALIA expedition onboard the R/V *Kilo Moana* and the global predicted bathymetry (v8.2) from *Smith and Sandwell* [1997]. (a) Overview map of the Samoa region including the Tonga Trench, the east-west oriented Vitiaz Lineament, and Wallis Island and Manua Seamount that (most likely) lay in a segment of the rather complex Lau Basin back-arc system. In this paper, Samoa is further divided into the "Western Samoan volcanic province" (WESAM) and the "Eastern Samoan volcanic province" (ESAM) based on geographic distribution. (b) Detailed bathymetric map of the ESAM province with two en echelon seamount trail segments depicting the morphogeochemical VAI and MALU trends. Both subtracks demonstrate a primary rift zone trending N110°E, and both seem to be emanating from Tutuila Island, which is unique among the Samoan Islands with its highly elongate primary rift zone that trends N70°E. We have indicated the dredge locations from the ALIA 2006 expedition if the samples were used in this study.

Samoa a truly intraplate hot spot and reduces the potential effects of plate tectonic boundary stresses on the formation of the older Samoan volcanoes in the WESAM province.

2.1. Western Samoan Volcanic Province

[9] The Western Samoan volcanic province (WESAM) includes mostly seamounts, shallow reefs or banks, and one island, which all lie west of Savai'i Island: Combe Reef, Waterwitch Bank, Siafiafi, Wallis Island, Lalla Rookh, Fa'aliga, Pasco, Field, Taviuni, Toafilemu, Toafe'ai and a large number of unnamed seamounts (Figure 1a). The WESAM is diffusely bordered to the south by the Vitiaz Lineament. These seamounts form a less well-defined linear pattern than the ESAM features, largely because this complex tectonized setting is characterized by horst and graben type features. In addition, the WESAM seamounts themselves are much broader than those in the ESAM, forming volcanic plateaus that sometimes are interconnected. The isotopic signature of the WESAM seamounts is similar to the EM2 signature in ESAM and based on previous studies the seamounts have ^{40}Ar/^{39}Ar ages more or less consistent with a 7.1 cm/yr plate motion model [*Hart et al.*, 2004].

2.2. Eastern Samoan Volcanic Province

[10] The Eastern Samoan volcanic province (ESAM) includes all volcanic islands and seamounts from Savai'i's western rift zone to the currently active Vailulu'u volcano. The islands that are discussed in this study include Savai'i, Upolu, Tutuila, Ofu/Olosega and Ta'u; newly age-dated seamounts include Tisa, Papatua, Tama'i, Soso, Muli (aka Northeast Bank), Tulaga, Malumalu, Vailulu'u and one unnamed seamount located on the eastern rift running between Tulaga and Tutuila (Figure 1a). Uo Mamae and Papatua are located south of the other features and do not seem to follow the same morphological trend. Further east, and in close proximity of Vailulu'u, lie two additional seamounts, Malulu seamount and Rose Atoll, that likely do not have the same origin as the other volcanoes in ESAM based on geochemical analysis [*Rodgers et al.*, 2003; *Jackson et al.*, 2010] and that seemingly are older based on several dredge hauls containing basaltic rocks with thick Mn crusts (AVON Leg 3 cruise in 1999 on board the R/V *Melville*). The HIMU and Rarotonga-like isotope signatures of these two seamounts seem to indicate that geochemically they may be related more

closely to one of the Cook-Austral-Rarotonga hot spots [*Jackson et al.*, 2010].

[11] ESAM also has a topographical arrangement with two short subparallel tracks of volcanic islands and seamounts that are trending somewhat obliquely within the overall Samoan lineament (Figure 1b). The subtracks are referred to as the MALU and VAI trends [*Hart et al.*, 2004; *Workman et al.*, 2004], whereby the MALU trend contains Malumalu, Tulaga, Tutuila and Tisa, and the VAI trend is located to the northeast and contains Vailulu'u, Ta'u, Ofu/Olosega, Muli, Soso and Tama'i. This en echelon arrangement can be compared to the subparallel Loa and Kea subtracks of the Hawaiian Emperor seamount trail, where the origination of these patterns have been explained by short episodes of compression in the lithosphere beneath Hawaii [e.g., *Jackson et al.*, 1972; *Jackson and Shaw*, 1975; *Jackson et al.*, 1975; *Natland*, 1980; *Shaw et al.*, 1980] and the sampling of a zonation in the Hawaiian mantle plume [e.g., *Abouchami et al.*, 2005; *Ren et al.*, 2005]. Recently, the Samoan subtracks have been proposed to be a result of northeastern plume motions as a response to the fast eastern rollback motion of the Tonga Trench, which seriously disrupted the mantle plume flow in the region over the last 1–2 Myr [*Hart et al.*, 2004].

2.3. Active Vailulu'u and Malumalu Volcanoes

[12] In the northern VAI subtrack volcanism starts at Tamai'i seamount and ends at Vailulu'u where all samples are less than a few hundred thousand years old, and most are less than 10 ka. An unobserved eruption took place November 2004 (±2 months), building the 300 m high Nafanua volcanic cone within the underwater crater of Vailulu'u [*Staudigel et al.*, 2006; *Sims et al.*, 2008]. The recent activity at Vailulu'u has been further highlighted by volcano-tectonic earthquakes emanating from an axial fault plane located inside the top of this volcanic structure and oriented parallel to its southeastern rift [*Konter et al.*, 2004], intense hydrothermal activity in and around its crater [*Hart et al.*, 2000; *Staudigel et al.*, 2004, 2006], and isotopic disequilibrium in the U-Th-Ra-Pa-Pb series for most of the dredge samples analyzed [*Sims et al.*, 2008]. As a result, Vailulu'u is now seen as the current locus of the Samoan mantle plume [*Hart et al.*, 2000, 2004; *Koppers et al.*, 2008].

[13] In the southern MALU subtrack, volcanism starts as an extension from Upolu Island and ends at Malumalu seamount, which has erupted several

times at <300 ka, <150 ka and <8 ka, based on observed excesses in ^{230}Th, ^{231}Pa and ^{226}Ra [*Sims et al.*, 2008]. This therefore gives two "active" or "zero-aged" volcanic centers at the easternmost end of the Samoan lineament, offset by only ~69 km (i.e., the measured distance between Vailulu'u and Malumalu).

2.4. Shield-Building Versus Posterosional Volcanism in Samoa

[14] Construction of Samoan volcanoes typically starts with an alkali-basalt-dominated shield-building stage, in contrast to the tholeiite-dominated Hawaiian shield-building stage, followed by one or more caldera collapses that are subsequently filled with more differentiated (postshield?) felsic lava flows [e.g., *Natland*, 1980]. After the caldera structures are filled, the volcano remains dormant for a period of time, is subject to erosion, and finally may experience a stage of posterosional or rejuvenated volcanism. The volcanic islands in ESAM are predominantly shield volcanoes, though the subaerial exposures on Savai'i and parts of Upolu and Tutuila are increasingly blanketed with posterosional lavas. Vailulu'u volcano, at the extreme eastern end of the chain, is currently active and still in an early shield-building stage, the islands of Ta'u, Olosega and Ofu consist of mildly eroded shield lavas, Tutuila Island has experienced advanced erosion of its shield and is covered with small amounts of posterosional material, Upolu Island is heavily eroded and approximately 1/3 covered with posterosional lava, whereas Savai'i Island is entirely resurfaced with these late stage lavas, but shield stage lavas may be exposed in the deepest stratigraphy in a gorge on the south side of the island [*Kear and Wood*, 1959; *Hart et al.*, 2000, 2004; *Workman et al.*, 2004; *Konter et al.*, 2010]. There are no K/Ar or ^{40}Ar/^{39}Ar age dates of the posterosional lavas from Upolu or Tutuila, although the Salani, Mulifanua and Lefaga formations on Upolu and the Leone formation on Tutuila appear to be postglacial and similar to the K/Ar-dated posterosional volcanics of Savai'i Island that are younger than 0.22 Ma [*McDougall*, 2010]. Some of this posterosional volcanism is exposed on Upolu in a series of small (uneroded) volcanic cones that formed along a near-linear east-west rift, spanning the width of the island and continuing in either direction over the full length of Savai'i to the west and onto parts of Tutuila to the east [*Natland and Winterer*, 2005]. Posterosional volcanics on subaerial Savai'i range in age from at least 0.39 Ma to less than 100 years old (i.e., historic eruptions occurred from 1905 to 1911 AD and ^{14}C ages range

from 2150 to 1830 BC to 1550–1820 AD), and erupted in numerous small volcanic cones, stretching out along its central rift zone [*Natland and Turner*, 1985; *Workman et al.*, 2004; *McDougall*, 2010; *Németh and Cronin*, 2009]. As these late stage volcanics have completely blanketed Savai'i Island, shield-building lava flows have only been observed on the deepest parts of its submarine flanks, with significantly older (approaching 5.0 Ma) ^{40}Ar/^{39}Ar ages [*Koppers et al.*, 2008].

2.5. VAI and MALU Geochemical Trends

[15] There are distinct Sr-Nd-Pb-O isotope and trace element characteristics that allow us to distinguish between posterosional (subaerial) volcanism on Savai'i, Tutuila and Upolu and the shield-building lavas collected elsewhere in the Samoan seamount trail [*Hart et al.*, 2004; *Workman et al.*, 2004; *Jackson et al.*, 2007a; *Workman et al.*, 2006, 2008; *Jackson et al.*, 2010]. Samoan shield lavas have ^{206}Pb/^{204}Pb ratios of 18.9–19.4 with corresponding ^{87}Sr/^{86}Sr ratios of 0.7044–0.72083 [*Wright and White*, 1986; *Workman et al.*, 2004; *Jackson et al.*, 2007a, 2010]. Posterosional lavas have lower ^{206}Pb/^{204}Pb values, whereby the ^{206}Pb/^{204}Pb ratio of ESAM posterosional basalts *increases* and the same ratio for shield-building basalts *decreases* with distance from the Vailulu'u hot spot location [*Hart et al.*, 2004]. In the same way, basalts from WESAM tend to *decrease* in ^{206}Pb/^{204}Pb with increasing distance (or age) from the hot spot [*Hart et al.*, 2004; *Workman et al.*, 2004]. These changes in Pb isotopic composition could be the result of a change in plume composition over time, a shift in melting proportions of the small-scale compositional diversity present in the plume, or changes in the interaction of the plume with the overriding Pacific lithosphere and/or asthenosphere. New isotopic evidence now indicates that the renowned EM2 pedigree of Samoa (e.g., highest ^{87}Sr/^{86}Sr and high ^{18}O in combination with low Ce/Pb and Nb/U ratios) is caused by a small admixture of ancient subducted continental-derived sediments [*White and Hofmann*, 1982; *Jackson et al.*, 2007a; *Workman et al.*, 2008]. Notably, the ESAM en echelon subtracks also have distinct isotopic signatures, whereby at a given ^{206}Pb/^{204}Pb ratio the MALU trend volcanoes have higher ^{208}Pb/^{204}Pb ratios compared to volcanoes in the VAI trend [*Workman et al.*, 2004]. Four seamounts (Combe, Alexa Bank, Lalla Rookh and Pasco Bank) that are located in WESAM have been analyzed and all plot within the trace element and Sr-Nd-Pb isotopic space with a "Samoan pedigree" [*Sinton et al.*, 1985; *Hart et al.*, 2004], and thus

may have the same volcanic origin as volcanoes from the ESAM. All above observations are confirmed by the latest WESAM and ESAM geochemical analyses [*Jackson et al.*, 2010].

3. The $^{40}Ar/^{39}Ar$ Dating Techniques

[16] In total we performed 36 new $^{40}Ar/^{39}Ar$ incremental heating analyses on 29 samples from 12 seamounts and the deep submarine flanks of most volcanic islands in the Samoa seamount trail. The results of these detailed incremental heating experiments are displayed in age plateau and isochron diagrams in Figures 2 and 3. Seamount locations and a summary of the $^{40}Ar/^{39}Ar$ ages are listed in Tables 1 and 2. The measurement data can be downloaded from the EarthRef.org Digital Archive (ERDA) and from the GEOCHRON online database as detailed in the auxiliary material.[1] The same data also are provided as ArArCALC files (in Microsoft Excel and PDF formats) in the auxiliary material.

3.1. Sample Preparation and Acid Leaching

[17] Three different sample types (groundmass, feldspar, biotite) were prepared for $^{40}Ar/^{39}Ar$ age analyses, each requiring a slightly different preparation. Preparation of the groundmass samples began by using a rock saw to remove visibly obvious alteration. Next, these samples were crushed using a porcelain jaw crusher and ground into three grain size fractions (500–300, 210–300 and <210 μm) using a stainless steel ring mill in short (1–2 s) intervals, interspersed by sieving. First, all material was ground and sieved until 90% was finer than 500 μm. Second, continuing using finer sieves, as much material as possible was ground into the <210 μm grain size fraction, with the goal to leave 25% in the 210–300 μm fraction. It is assumed that this grinding process concentrates less altered (and harder) basalt grains in the coarser 210–300 μm size fraction. The 210–300 μm size fraction was then rinsed several times with water, finished with a final rinse using 18 MΩ water and set in an 40°C oven to dry overnight. Next the groundmass samples were run through a Frantz magnetic separator at a series of increasing amperages. The magnetic portions collected at each amperage setting were examined under a microscope and the best (based on sample purity) was selected to be cleaned by acid leaching in 1 N HCl (60 min), 6 N HCl (60 min), 1 N HNO3 (60 min) and 18 MΩ water (60 min). Each acid

step (and water step) was conducted in an ultrasonic bath heated to 50°C. The samples were rinsed with 18 MΩ water a final time and dried overnight in an oven at 40°C for a second time. Last, the groundmass samples were handpicked using a binocular microscope to remove any grains containing (remaining) alteration or parts of phenocrysts and microcrysts. Approximately 100 mg of groundmass material was collected from each sample for the $^{40}Ar/^{39}Ar$ dating of which typically 50 mg was used in the analysis. In cases of more severe alteration present in the samples, the acid leaching procedure was repeated to ensure a thorough removal of all microscopically visible alteration minerals.

[18] The biotite samples were prepared the same way as the groundmass samples, all the way through the steps to sieve for grain size. Both the 500–300 and 210–300 μm fractions were rinsed in 18 MΩ water, but *not* acid leached, and dried overnight in a 40°C oven. The biotite samples were run through the Frantz magnetic separator at several different amperages to identify the fraction most concentrated in biotite. The biotite fraction selected was then placed in 18 MΩ water again and put in an ultrasonic bath heated to 50°C for 60 min. This procedure was repeated three times, samples were rinsed a final time with 18 MΩ water, and placed in a 40°C oven to dry overnight. Finally, the biotite samples were handpicked to separate biotite grains from grains that still showed some adhering groundmass material. Approximately 10 mg of biotite was collected from each sample.

[19] The feldspar samples were initially prepared the same as the groundmass and biotite samples, except after sieving *all* three grain size fractions were rinsed and dried overnight in an oven at 40°C. Each fraction was run through the Frantz magnetic separator. The nonmagnetic portion of the sample remaining after the magnet was run at its maximum amperage typically contained most of the unaltered feldspar grains and was further cleaned by acid leaching. The feldspar samples were leached in 1 N HCl (60 min), 6 N HCl (60 min), 1 N HNO3 (60 min), 5% HF (15 min), 1 N HNO3 (30 min) and 18 MΩ water (60 min) in a 50°C ultrasonic bath. The feldspar samples were then rinsed (three times) in 18 MΩ water and placed in a 40°C oven to dry overnight. Finally, the samples were handpicked to remove any altered feldspar grains or feldspar grains partly holding pieces of other minerals or groundmass. Approximately 35 mg of feldspar was collected from each sample.

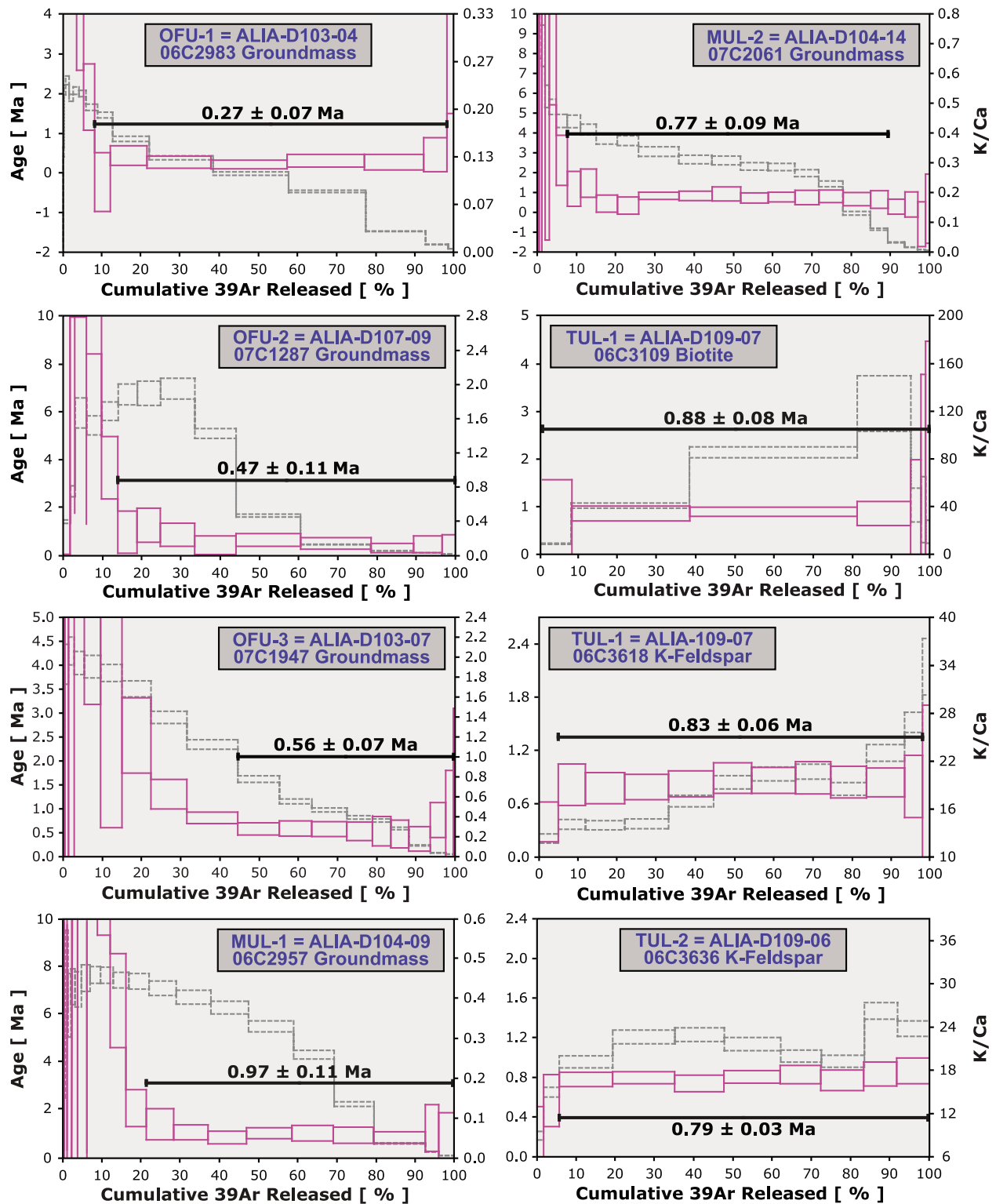**Figure 2.** High-resolution incremental heating ^{40}Ar/^{39}Ar age spectra for Samoan seamount trail basalts. The reported ^{40}Ar/^{39}Ar ages are weighted age estimates with errors reported on the 95% confidence level, including 0.3%–0.4% standard deviations in the J value. All samples where monitored against FCT-3 biotite (28.03 ± 0.18 Ma, 1σ) as calibrated by *Renne et al.* [1998]. Data are listed in Table 2, and ArArCALC age calculation files can be downloaded from the EarthRef.org Digital Archive (ERDA) and GEOCHRON as described in the auxiliary material. Pink lines are ^{40}Ar/^{39}Ar ages, and gray lines are K/Ca ratios.
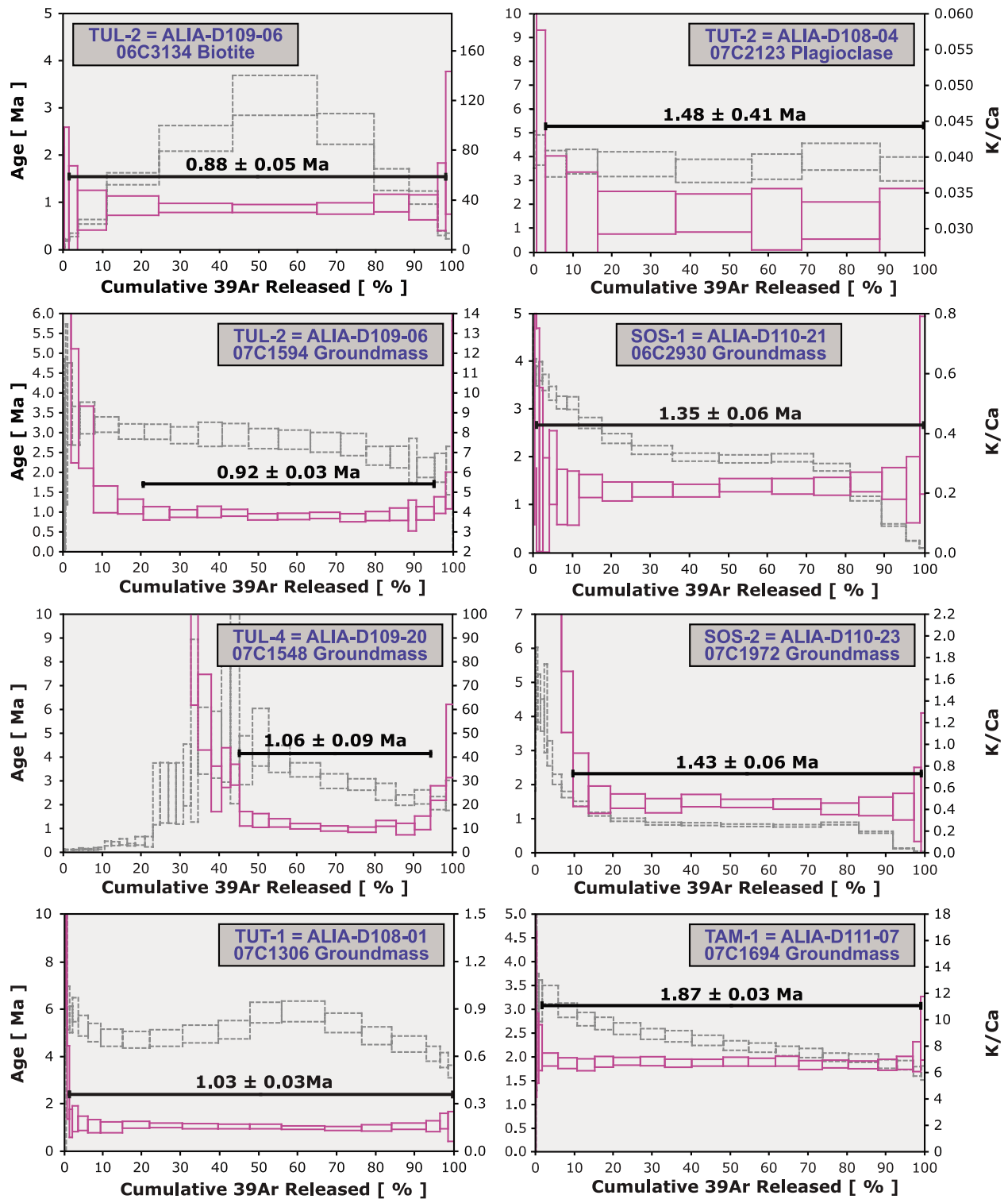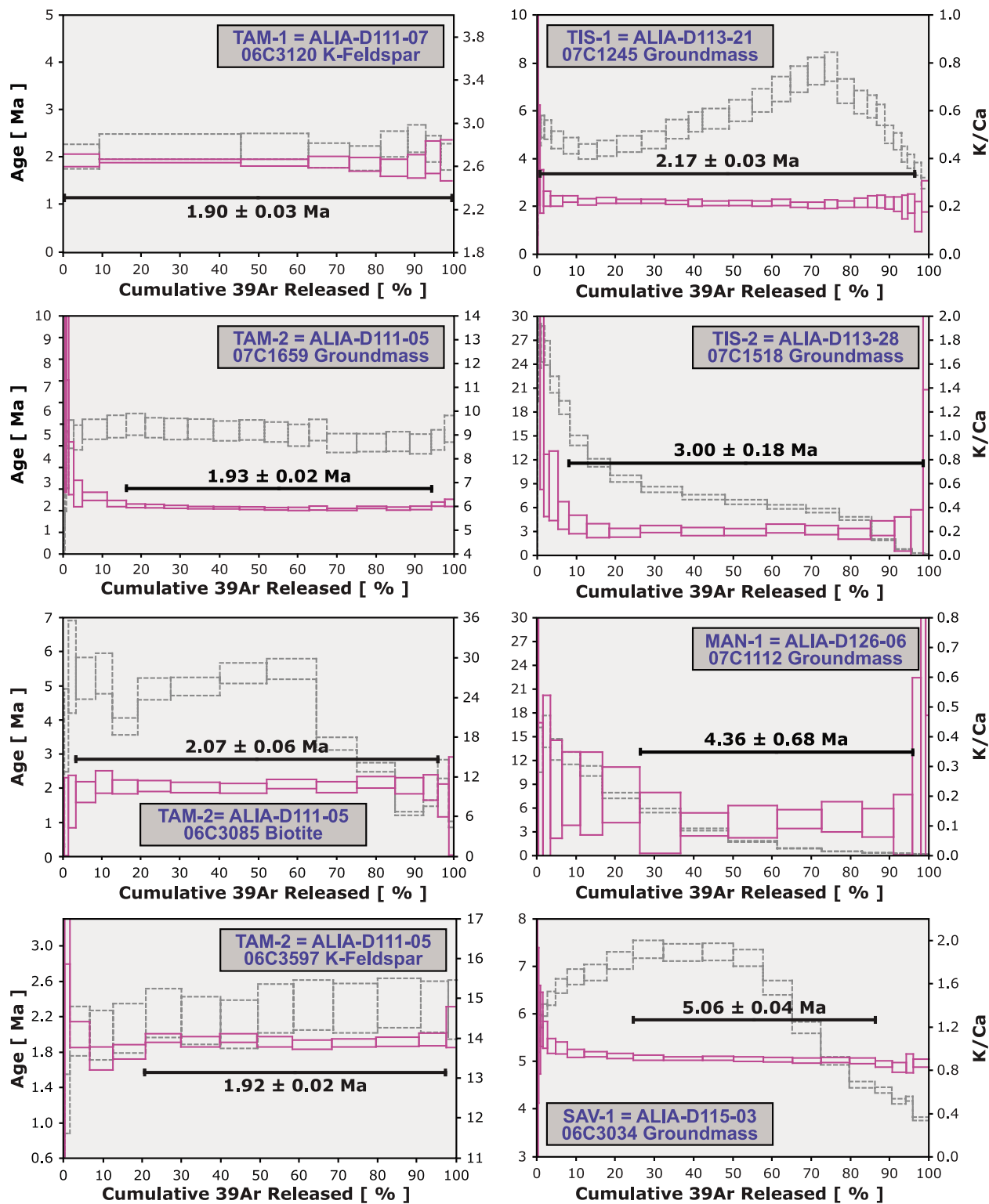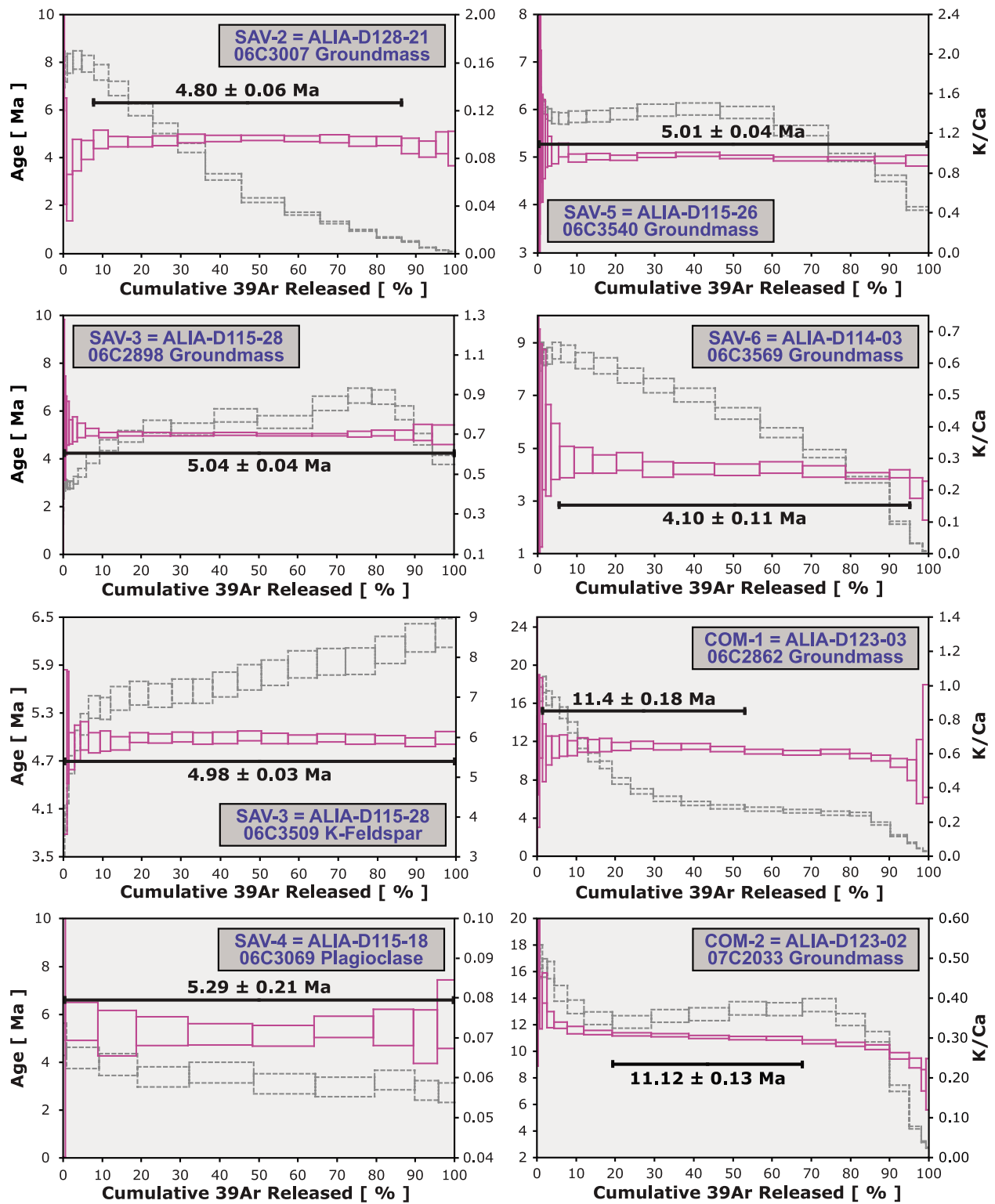
Figure 2. (continued)
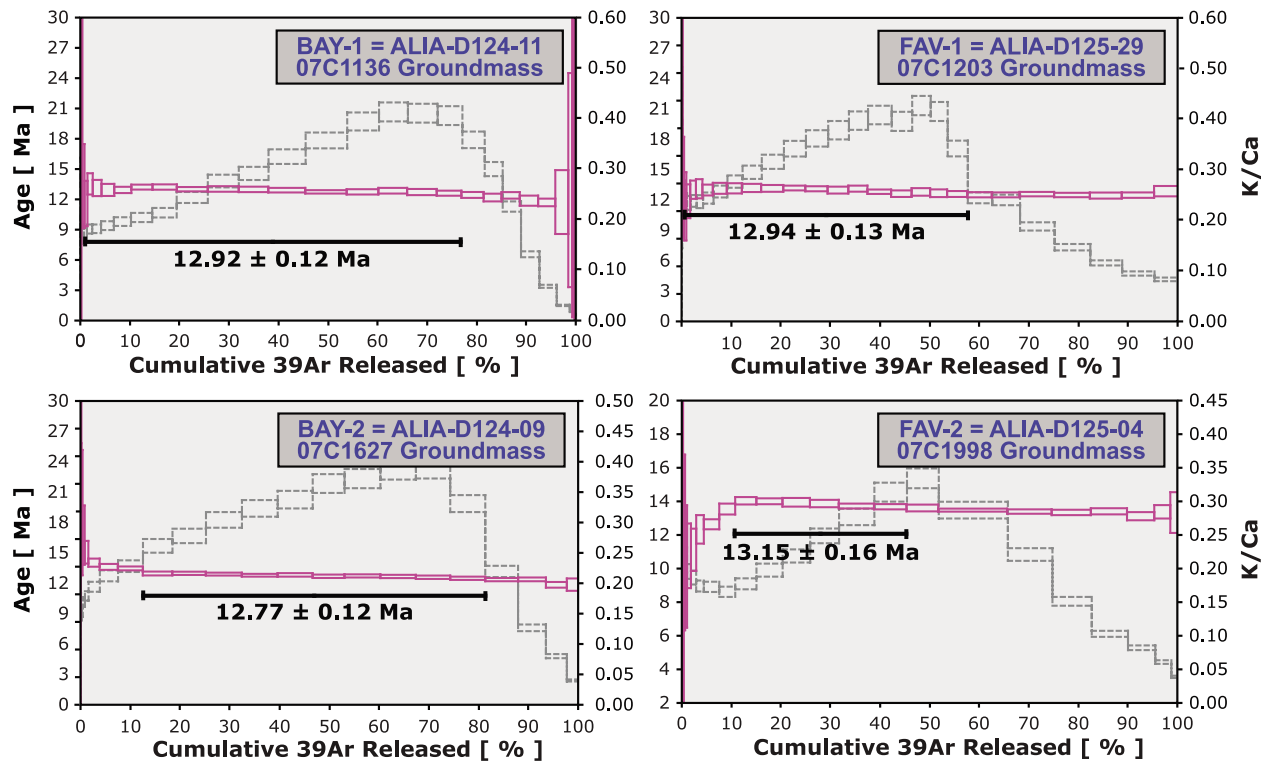
Figure 2. (continued)

Figure 2. (continued)

Figure 2. (continued)

3.2. The $^{40}Ar/^{39}Ar$ Mass Spectrometry and Age Calculations

[20] Following sample preparation and hand picking the samples were irradiated for 6–7 h in the TRIGA CLICIT nuclear reactor at Oregon State University. Each sample was wrapped in aluminum foil, folded to form thin disks, and placed in a vacuum-sealed quartz cylinder with the FCT-3 biotite (28.03 ± 0.18 Ma, 1σ) standard flux monitor [Renne et al., 1998] at the top and bottom and at intermittent heights throughout this cylinder. Individual J values for each sample were calculated by parabolic extrapolation of the measured flux gradient against irradiation height in the cylinder. The $^{40}Ar/^{39}Ar$ incremental heating age determinations were performed using a continuous 10 W CO_2 laserprobe combined with a MAP-215/50 mass spectrometer at Oregon State University. The mass spectrometer is a 90° sector instrument with a Nier-type source with an all-metal gas extraction system. It has an electron multiplier for high sensitivity and an electrostatic analyzer with adjustable collector slit for an effective resolution (~600) of Ar peaks from small hydrocarbon peaks. Irradiated samples were loaded into Cu planchettes designed with a variety of pans (holding up to 50 mg of material) that were pumped within a sample chamber fitted with a ZnS window transparent to the CO_2 laser wavelength. Software allowed for scanning across samples in preset patterns with a defocused laser beam, to evenly heat the geological materials. After heating, the released gas was entered into an ultraclean extraction line where reactive gases were removed using an SAES Zr-Al ST101 GP50 getter operated at 400°C for ~15 min, followed by a final cleaning for ~5 min using two SAES Fe-V-Zr ST172 getters operated at 200°C and room temperature. All ages were calculated using the corrected Steiger and Jäger [1977] decay constant of $5.530 \pm 0.097 \times 10^{-10}$ 1/yr (2σ) as reported by Min et al. [2000]. For a detailed description of the analytical facility and the constants used in the age calculations we refer to Table 2 in the work by Koppers et al. [2003]. Incremental heating plateau ages and isochron ages were calculated as weighted means with $1/\sigma^2$ as weighting factor [Taylor, 1997] and as YORK2 least squares fits with correlated errors [York, 1968] using the ArArCALC v2.5 software from Koppers [2002] that is available from the http://earthref.org/tools/ararcalc.htm website. In this paper, all errors on the $^{40}Ar/^{39}Ar$ ages are reported at the 95% confidence level (2σ), unless otherwise indicated, including typical 0.3%–0.5% uncertainties in the J value.

[21] Many heating steps were done on each sample to ensure even heating and complete argon outgassing (7–16 steps for biotite, 9–22 steps for
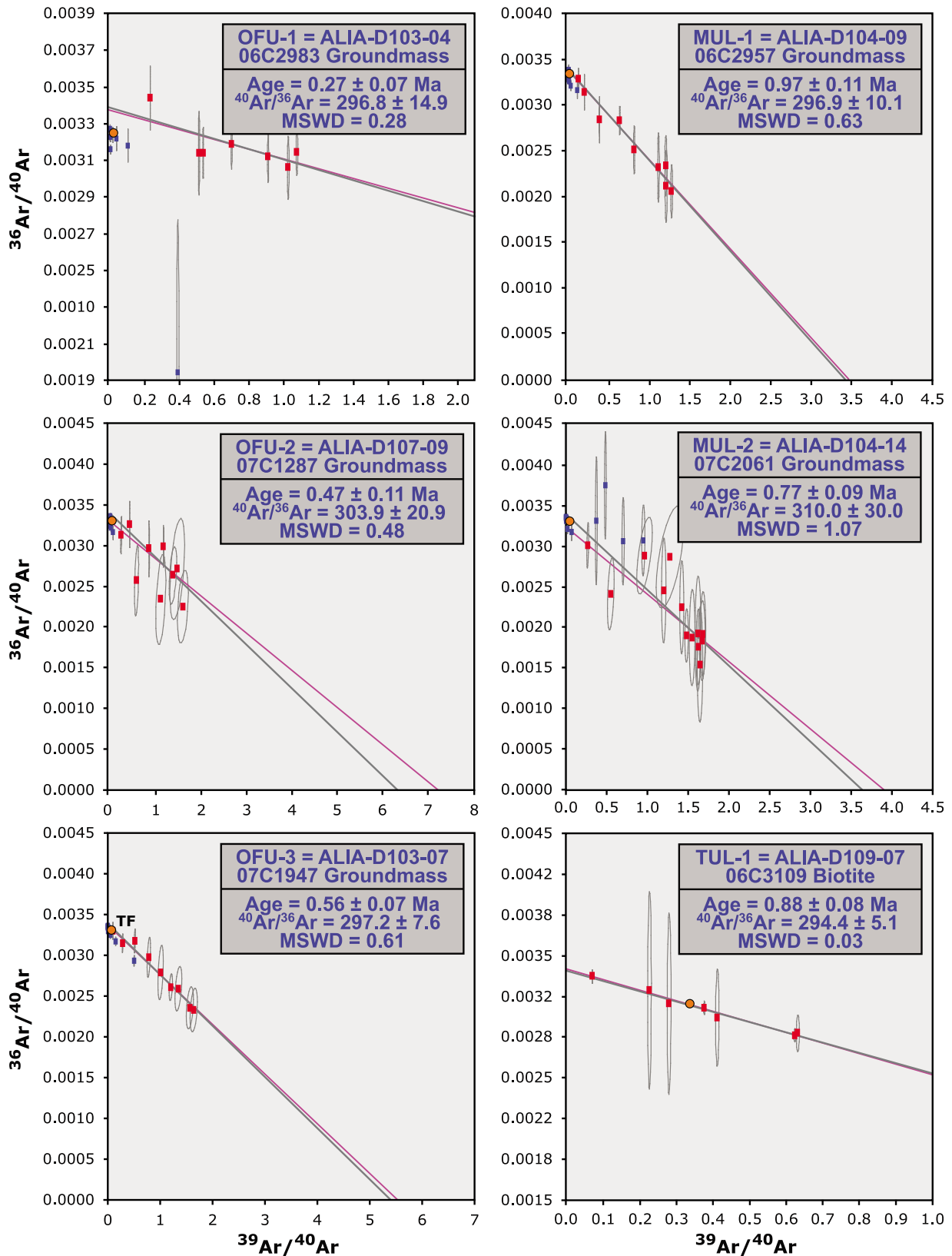
Figure 3

feldspars and 16–26 steps for groundmass samples). Also, increased numbers of very low temperature heating steps were conducted at laser intensities below 0.05 W to ensure an effective removal of alteration and atmospheric signatures. Before beginning a sample, and after every three heating steps, system blanks were measured, which were used to estimate interpolated background values against measurement time for each of the incremental heating steps. The data peak intensities were reduced using linear or exponential curve fits with respect to the inlet time of the gas sample into the mass spectrometer. Total fusion ages were calculated using the ArArCALC software. In this calculation, all heating steps are added up (recombined), giving an age as if all argon gas was released at once in a single fusion. If the total fusion values fall on the isochrons, for example, it indicates that their systems have remained closed and there was no loss or addition of argon since the eruption of the submarine basalts, even if internal redistribution(s) occurred. Plateau ages and isochrons with MSWDs higher than 1 were taken to indicate an increased scatter due to geological uncertainties beyond the precision of the individual increment ages themselves. In these cases, the reported analytical errors are multiplied by the $\sqrt{MSWD}$ [*York*, 1968; *Kullerud*, 1991].

3.3. Quality Criteria and Groundmass $^{40}Ar/^{39}Ar$ Age Dating

[22] In this study, we have adopted four criteria to determine the reliability of the $^{40}Ar/^{39}Ar$ ages [*Lanphere and Dalrymple*, 1976; *Fleck et al.*, 1977; *Pringle*, 1993]: (1) high-temperature plateaus in the age spectra should include more than three incremental heating steps and at least 50% of the total amount of $^{39}Ar_K$ released; (2) the plateau and isochron ages should be concordant at the 95% confidence level; (3) the $^{40}Ar/^{36}Ar$ intercepts on the isochron diagrams should be concordant with the atmospheric value of 295.5 at the 95% confidence level; and (4) the mean square of weighted deviations (MSWD [*York*, 1968; *Roddick*, 1978]) for plateau and isochron ages should be sufficiently

small when compared to student's t test and F statistic critical values for significance, respectively.

[23] We emphasize here that these four criteria were used as guidelines for the reliability of data only, and that careful examinations of the age systematics were conducted before making final conclusions about the crystallization age of our samples, as these criteria are not appropriate for the evaluation of altered groundmass separates in all cases [*Koppers et al.*, 2000]. It has long been recognized that submerged volcanic rocks undergo (severe) hydrothermal alteration and seawater weathering, processes that may add or leach out potassium, remove radiogenic $^{40}Ar*$ and recrystallize parts of the rocks [*Hart*, 1969; *Kaneoka*, 1972; *Fleck et al.*, 1977; *Seidemann*, 1977; *Roddick*, 1978; *Seidemann*, 1978, 1988]. Additionally, large phenocrysts of olivine and pyroxene in basaltic rocks likely have excess (mantle-derived) argon and should be avoided by focusing on the analyses of groundmass as an alternative to whole rock age dating of phyric basalts. Recoil of argon isotopes produced during irradiation [*Turner and Cadogan*, 1974; *Dalrymple and Clague*, 1976; *Huneke*, 1976; *Huneke and Smith*, 1976; *Seidemann*, 1978; *Walker and McDougall*, 1982] may be responsible for the loss of $^{39}Ar_K$ and $^{37}Ar_{Ca}$ in fine grained (alteration) minerals and causes both high [*Huneke*, 1976] and low apparent ages in the $^{40}Ar/^{39}Ar$ age spectra [*Davis et al.*, 1989; *Pringle*, 1993; *Koppers et al.*, 2000]. When alteration in seamount basalts is severe, especially for older seamounts, some very fine grained alteration minerals often remain present in the groundmass samples, even following the intensive acid-leaching procedures carried out during our sample preparation. This remaining alteration is the very source of the sometimes significant recoil effects evident in our age spectra, typically causing high apparent ages at low temperatures, low apparent ages at high temperatures, and often a mild sloping of the age plateaus. However, as we will show in this paper, with careful sample preparation and high-resolution incremental heating analyses we can achieve credible, reproducible age data for seamount basalts [*Nauert and Gans*, 1994; *Sharp*

Figure 3. High-resolution incremental heating $^{40}Ar/^{39}Ar$ isochron analyses on crystalline groundmass samples and plagioclase or biotite mineral separates for Samoan seamount trail basalts. Note that "reference lines" (dark gray) are shown (defined by the 295.5 atmospheric intercept on the $^{36}Ar/^{40}Ar$ axis and by the plateau age on the $^{39}Ar/^{40}Ar$ axis) in conjunction with the calculated isochrons (pink). Red squares indicate the steps included in the age calculations. The locations of the total fusion (TF) points are indicated by orange circles (not included in the calculations). Data are listed in Table 2, and ArArCALC age calculation files can be downloaded from the EarthRef.org Digital Archive (ERDA) and GEOCHRON as described in the auxiliary material. Samples that were "too radiogenic" (Table 2) have not been included, but these diagrams can be found in electronic form in the age calculation files in the auxiliary material.
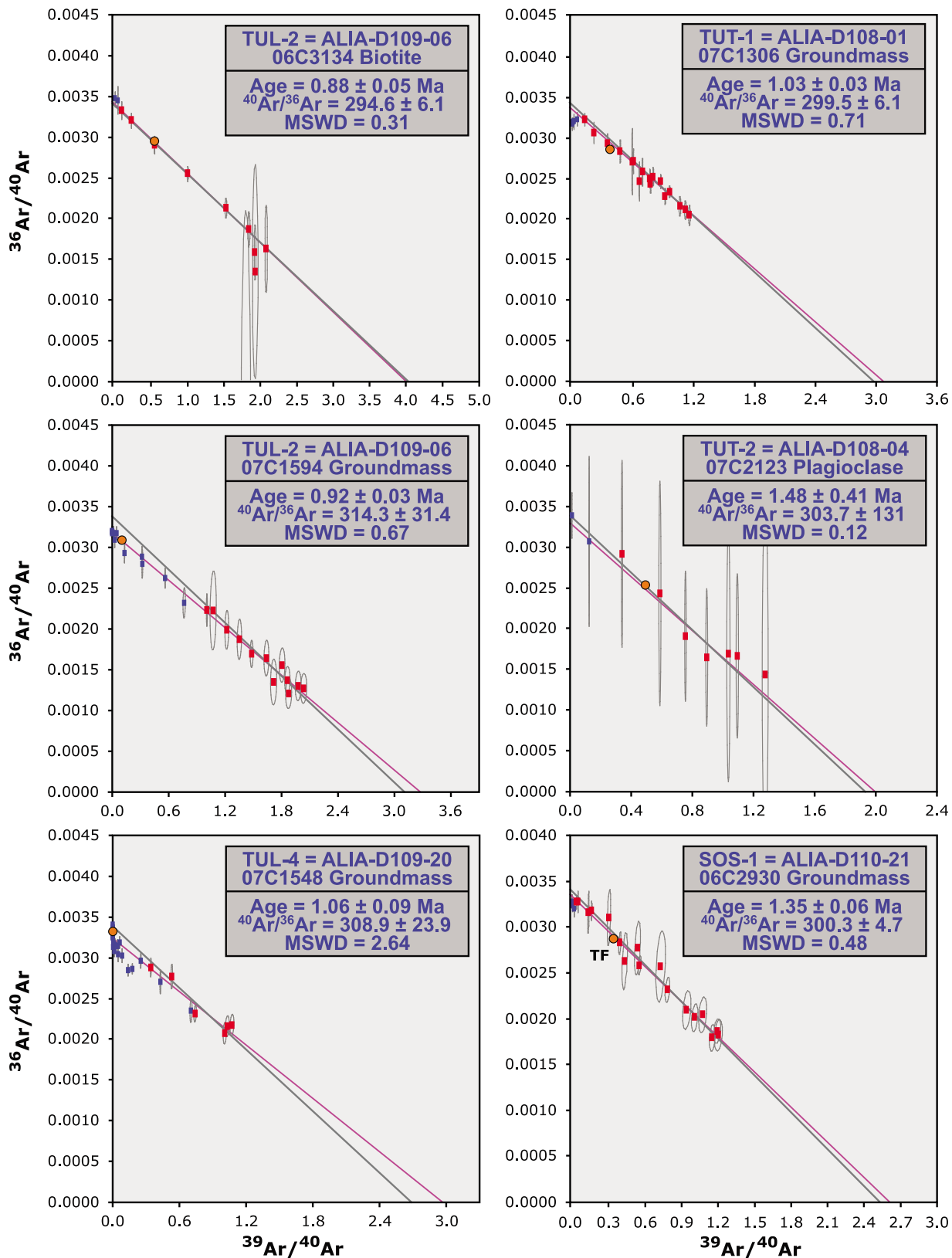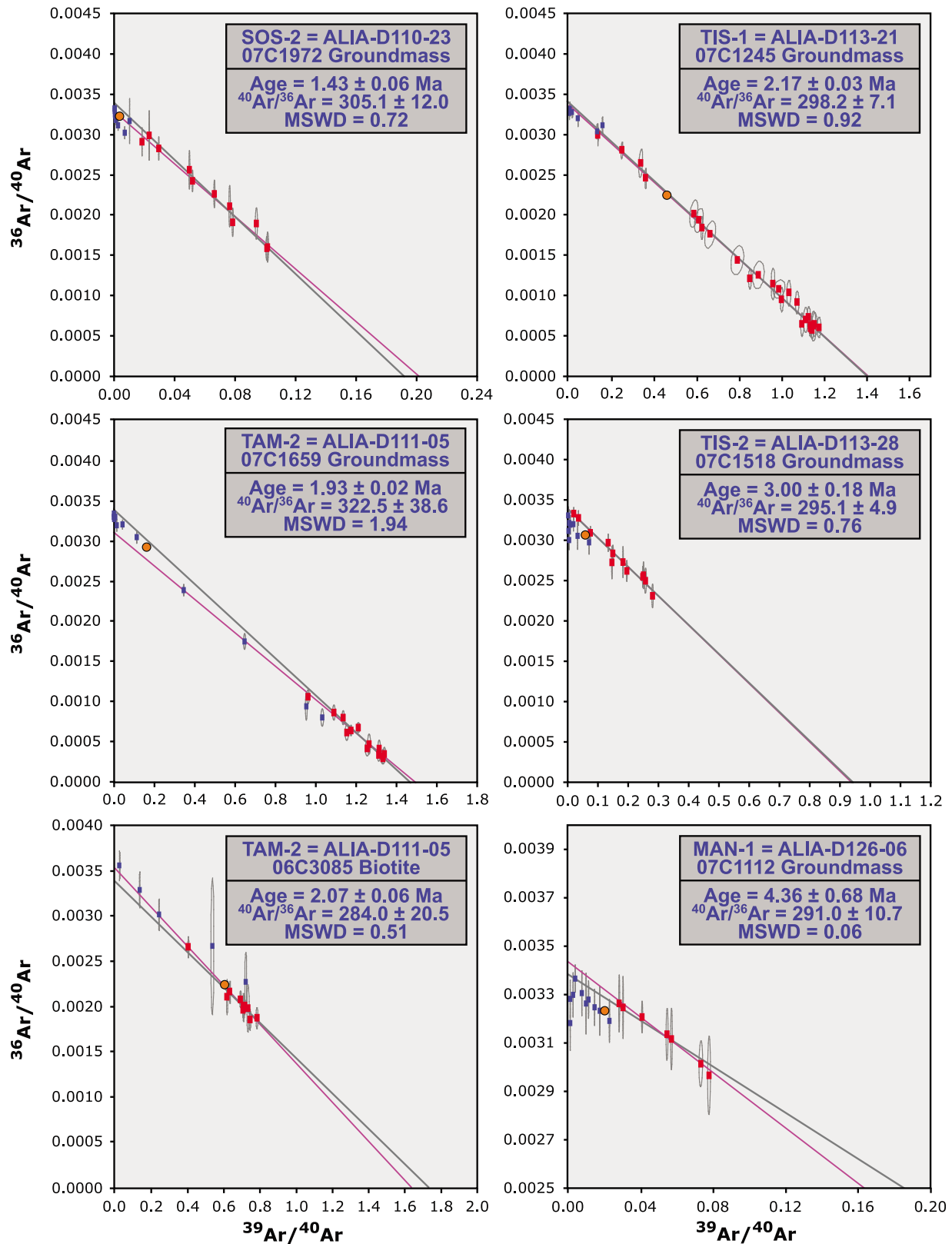
Figure 3. (continued)

SOS-2 = ALIA-D110-23
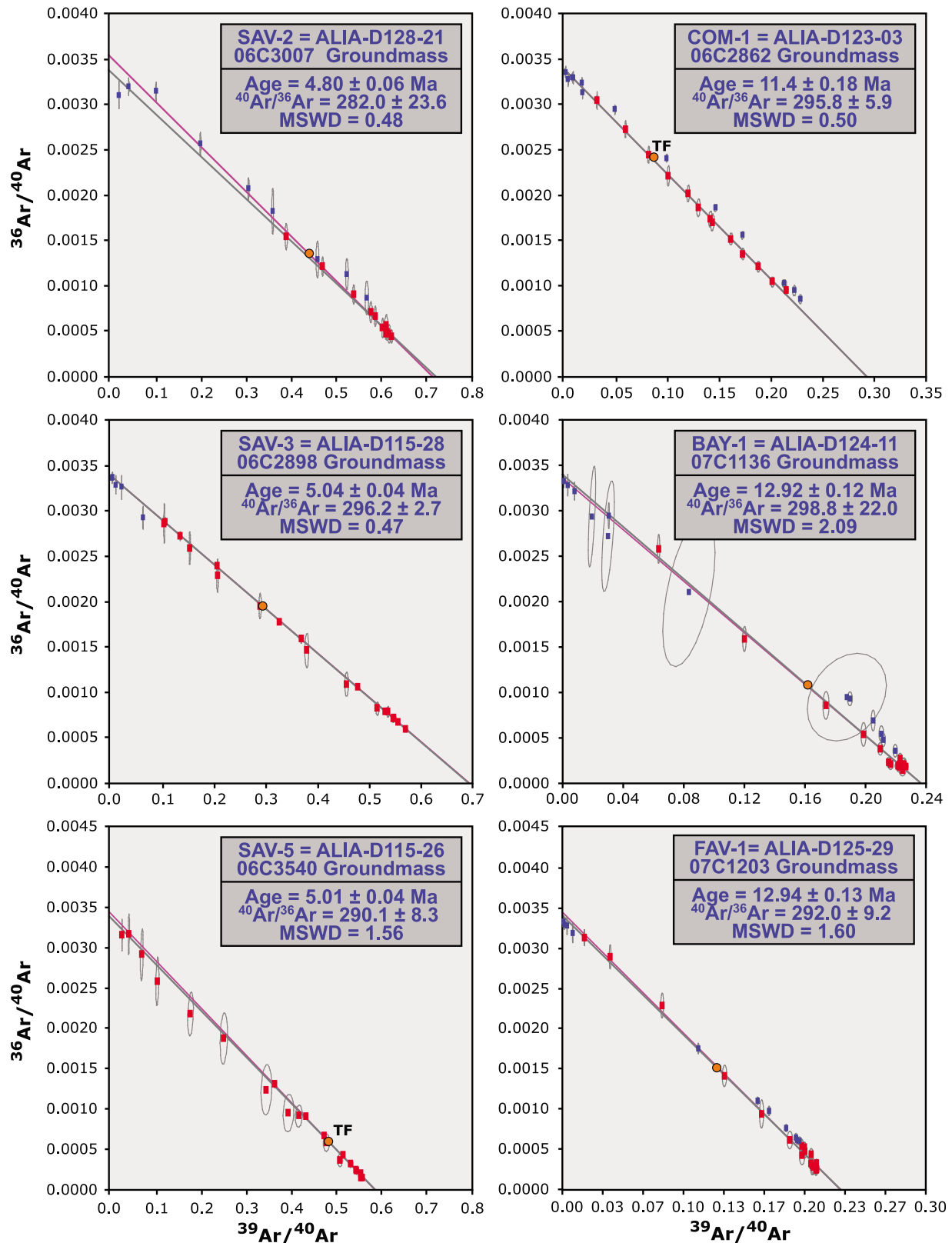**07C1972 Groundmass**
Age = 1.43 ± 0.06 Ma
$^{40}Ar/^{36}Ar$ = 305.1 ± 12.0
MSWD = 0.72

TIS-1 = ALIA-D113-21
07C1245 Groundmass
Age = 2.17 ± 0.03 Ma
$^{40}Ar/^{36}Ar$ = 298.2 ± 7.1
MSWD = 0.92

TAM-2 = ALIA-D111-05
07C1659 Groundmass
Age = 1.93 ± 0.02 Ma
$^{40}Ar/^{36}Ar$ = 322.5 ± 38.6
MSWD = 1.94

TIS-2 = ALIA-D113-28
07C1518 Groundmass
Age = 3.00 ± 0.18 Ma
$^{40}Ar/^{36}Ar$ = 295.1 ± 4.9
MSWD = 0.76

TAM-2 = ALIA-D111-05
06C3085 Biotite
Age = 2.07 ± 0.06 Ma
$^{40}Ar/^{36}Ar$ = 284.0 ± 20.5
MSWD = 0.51

MAN-1 = ALIA-D126-06
07C1112 Groundmass
Age = 4.36 ± 0.68 Ma
$^{40}Ar/^{36}Ar$ = 291.0 ± 10.7
MSWD = 0.06

Figure 3.   (continued)

Figure 3.   (continued)

Table 1. Sample Locations in the Samoa Seamount Trail[a]

Sample	Lab Code	Seamount Name	Latitude	Longitude	Depth (mbsl)
Alia 103-04	OFU-1	Ofu Island: West Rift	14°06.1′S	169°54.3′E	1850–2230
Alia 107-09	OFU-2	Ofu Island: South Rift	14°10.3′S	169°40.0′E	2395–2585
Alia 103-07	OFU-3	Ofu Island: West Rift	14°06.1′S	169°54.3′E	1850–2230
Alia 104-09	MUL-1	Muli Seamount	14°01.1′S	170°11.3′E	2000–2505
Alia 104-14	MUL-2		14°01.1′S	170°11.3′E	2000–2505
Alia 109-07	TUL-1	Tulaga Ridge	14°39.1′S	170°01.4′E	2460–2930
Alia 109-07	TUL-1		14°39.1′S	170°01.4′E	2460–2930
Alia 109-06	TUL-2		14°39.1′S	170°01.4′E	2460–2930
Alia 109-06	TUL-2		14°39.1′S	170°01.4′E	2460–2930
Alia 109-06	TUL-2		14°39.1′S	170°01.4′E	2460–2930
Alia 109-20	TUL-4		14°39.1′S	170°01.4′E	2460–2930
Alia 108-01	TUT-1	Rift between Tutuila-Tulaga	14°28.2′S	170°18.0′E	2750–3450
Alia 108-04	TUT-2		14°28.2′S	170°18.0′E	2750–3450
Alia 110-21	SOS-1	Soso Seamount	13°46.1′S	170°14.5′E	1805–1995
Alia 110-23	SOS-2		13°46.1′S	170°14.5′E	1805–1995
Alia 111-07	TAM-1	Tamai'i Seamount	13°45.3′S	170°32.1′E	2705–2845
Alia 111-07	TAM-1		13°45.3′S	170°32.1′E	2705–2845
Alia 111-05	TAM-2		13°45.3′S	170°32.1′E	2705–2845
Alia 111-05	TAM-2		13°45.3′S	170°32.1′E	2705–2845
Alia 111-05	TAM-2		13°45.3′S	170°32.1′E	2705–2845
Alia 113-21	TIS-1	Tisa Seamount	14°25.9′S	171°19.9′E	1625–2685
Alia 113-28	TIS-2		14°25.9′S	171°19.9′E	1625–2685
Alia 126-06	MAN-1	Manuta Island	13°18.0′S	179°18.0′E	925–1400
Alia 115-03	SAV-1	Savai'i Island	14°05.5′S	172°56.5′E	3200–3245
Alia 128-21	SAV-2		13°12.7′S	172°05.8′E	2550–2575
Alia 115-28	SAV-3		14°05.5′S	172°56.5′E	3200–3245
Alia 115-28	SAV-3		14°05.5′S	172°56.5′E	3200–3245
Alia 115-18	SAV-4		14°05.5′S	172°56.5′E	3200–3245
Alia 115-26	SAV-5		14°05.5′S	172°56.5′E	3200–3245
Alia 114-03	SAV-6		13°58.7′S	172°44.4′E	2470–2510
Alia 123-03	COM-1	Combe Seamount	12°44.9′S	177°22.1′E	2250–2885
Alia 123-02	COM-2		12°44.9′S	177°22.1′E	2250–2885
Alia 124-11	BAY-1	Bayonaise Seamount	12°36.0′S	179°18.0′E	2660–2730
Alia 124-09	BAY-2		12°36.0′S	179°18.0′E	2660–2730
Alia 125-29	FAV-1	Favavesi Seamount	12°39.0′S	179°12.0′E	2010–2465
Alia 125-04	FAV-2		12°39.0′S	179°12.0′E	2010–2465

[a]The samples used in this study were dredged in 2005 during the ALIA expedition using the R/V *Kilo Moana* (KM0506). See http://earthref.org/ERESE/projects/ALIA/for details.

et al., 1996; *Koppers et al.*, 2000; *O'Connor et al.*, 2001; *Sharp and Clague*, 2006; *Koppers et al.*, 2007; *O'Connor et al.*, 2007; *Koppers et al.*, 2008].

3.4. Age Reproducibility

[24] To show that we can effectively bypass most of the alteration signatures in groundmass samples, and thus produce reproducible $^{40}Ar/^{39}Ar$ crystallization ages for the Samoan seamount basalts, we performed *duplicate analyses* in four instances from comagmatic phenocrystic phases of feldspar and biotite (Table 2). In two samples this resulted in the matching ages within the margin of error (ALIA D115-28, D109-07). In the other two cases the ages have small 0.02–0.06 Ma 2σ uncertainty estimates (ALIA D111-05, D109-06) with the groundmass being concordant with one comagmatic mineral phase and having minor offsets up to 0.15 Ma to

the second mineral phase. The reproducibility is also excellent between different basaltic samples from the same dredge site, as is shown in three groundmass analyses for dredge ALIA D115 on the deep flanks of Savai'i Island with plateau ages of 5.07 ± 0.04, 5.04 ± 0.04 and 5.01 ± 0.04 Ma [*Koppers et al.*, 2008]. These reproducible results provide further credence for the accuracy of these high-precision ages.

4. The $^{40}Ar/^{39}Ar$ Results

[25] In 2005, the ALIA expedition (http://earthref.org/ERESE/projects/ALIA) collected dredge samples from the deep submarine flanks of the Samoan islands and seamounts in an attempt to sample the initial, shield-building volcanism of the archipelago. The dredge samples recovered relatively unaltered

Table 2. Incremental Heating ^{40}Ar/^{39}Ar Analyses on the Samoa Seamount Trail[a]

Sample	Lab Code	Experiment	Sample Type	Age Spectrum					Total Fusion:	Inverse Isochron Analyses		
				Age ± 2σ (Ma)	^{39}Ar (%)	K/Ca	MSWD	n	Age ± 2σ (Ma)	Age ± 2σ (Ma)	^{40}Ar/^{36}Ar Intercept	MSWD
Alia 103-04	OFU-1	06C2983	Groundmass	0.27 ± 0.14	90	0.017	0.24	7	4.37 ± 0.75	0.26 ± 0.28	296.8 ± 29.7	0.28
Alia 107-09	OFU-2	07C1287	Groundmass	0.49 ± 0.21	86	0.017	0.38	9	5.47 ± 2.25	0.42 ± 0.29	305.5 ± 40.6	0.42
Alia 103-07	OFU-3	07C1947	Groundmass	0.56 ± 0.07	55	0.037	0.56	9	2.65 ± 0.68	0.55 ± 0.09	297.2 ± 7.6	0.61
Alia 104-09	MUL-1	06C2957	Groundmass	0.97 ± 0.11	78	0.011	0.57	9	6.70 ± 2.63	0.95 ± 0.15	296.9 ± 10.1	0.63
Alia 104-14	MUL-2	07C2061	Groundmass	0.77 ± 0.09	82	0.159	1.12	13	1.76 ± 0.40	0.71 ± 0.14	310.0 ± 30.0	1.07
Alia 109-07	TUL-1	06C3109	Biotite	0.88 ± 0.08	100	10.763	0.06	7	0.86 ± 0.11	0.90 ± 0.13	294.4 ± 5.1	0.03
Alia 109-07	TUL-1	06C3618	K feldspar	0.83 ± 0.06	94	17.122	0.22	10	0.81 ± 0.06	too radiogenic	too radiogenic	too radiogenic
Alia 109-06	TUL-2	06C3636	K feldspar	0.79 ± 0.03	95	21.429	0.66	8	0.77 ± 0.03	too radiogenic	too radiogenic	too radiogenic
Alia 109-06	TUL-2	06C3134	Biotite	0.88 ± 0.05	98	18.385	0.28	9	0.86 ± 0.09	0.89 ± 0.07	294.6 ± 6.1	0.31
Alia 109-06	TUL-2	07C1594	Groundmass	0.92 ± 0.03	74	7.419	0.76	12	2.47 ± 0.18	0.88 ± 0.08	314.3 ± 31.4	0.67
Alia 109-20	TUL-4	07C1548	Groundmass	1.06 ± 0.09	36	26.729	2.82	6	31.37 ± 9.22	0.96 ± 0.20	308.9 ± 23.9	2.64
Alia 108-01	TUT-1	07C1306	Groundmass	1.04 ± 0.03	99	0.709	0.79	17	1.29 ± 0.07	1.00 ± 0.06	299.5 ± 6.1	0.72
Alia 108-04	TUT-2	07C2123	Plagioclase	1.48 ± 0.41	97	0.039	0.11	7	1.46 ± 0.48	1.44 ± 0.82	303.7 ± 131	0.12
Alia 110-21	SOS-1	06C2930	Groundmass	1.35 ± 0.06	99	0.027	0.71	17	1.52 ± 0.09	1.31 ± 0.07	300.3 ± 4.7	0.48
Alia 110-23	SOS-2	07C1972	Groundmass	1.43 ± 0.06	89	0.023	0.92	11	3.96 ± 0.46	1.36 ± 0.11	305.1 ± 12.0	0.72
Alia 111-07	TAM-1	07C1694	Groundmass	1.87 ± 0.03	97	7.909	0.45	17	1.89 ± 0.03	too radiogenic	too radiogenic	too radiogenic
Alia 111-07	TAM-1	06C3120	K feldspar	1.90 ± 0.03	100	2.746	0.62	9	1.89 ± 0.04	too radiogenic	too radiogenic	too radiogenic
Alia 111-05	TAM-2	07C1659	Groundmass	1.93 ± 0.02	78	9.034	2.15	13	2.41 ± 0.10	1.90 ± 0.05	322.5 ± 38.6	1.94
Alia 111-05	TAM-2	06C3085	Biotite	2.07 ± 0.06	93	10.170	0.57	11	2.01 ± 0.06	2.19 ± 0.22	284.0 ± 20.5	0.51
Alia 111-05	TAM-2	06C3597	K feldspar	1.92 ± 0.02	77	14.679	1.09	8	1.91 ± 0.02	too radiogenic	too radiogenic	too radiogenic
Alia 113-21	TIS-1	07C1245	Groundmass	2.18 ± 0.03	96	0.519	0.93	25	2.23 ± 0.05	2.17 ± 0.04	298.2 ± 7.1	0.94
Alia 113-28	TIS-2	07C1518	Groundmass	3.00 ± 0.18	91	0.031	0.69	12	4.64 ± 0.38	3.02 ± 0.27	295.1 ± 4.9	0.76
Alia 126-06	MAN-1	07C1112	Groundmass	4.36 ± 0.68	70	0.010	0.16	7	6.78 ± 1.11	5.15 ± 1.99	291.0 ± 10.7	0.06
Alia 115-03	SAV-1	06C3034	Groundmass	5.07 ± 0.04	68	1.124	1.60	9	5.10 ± 0.04	too radiogenic	too radiogenic	too radiogenic
Alia 128-21	SAV-2	06C3007	Groundmass	4.80 ± 0.06	79	0.224	0.55	11	4.70 ± 0.07	4.84 ± 0.10	282.0 ± 23.6	0.48
Alia 115-28	SAV-3	06C2898	Groundmass	5.04 ± 0.04	100	0.580	0.46	19	5.07 ± 0.05	5.03 ± 0.04	296.2 ± 2.7	0.47
Alia 115-28	SAV-3	06C3509	K feldspar	4.98 ± 0.03	100	6.496	0.54	21	4.97 ± 0.03	too radiogenic	too radiogenic	too radiogenic
Alia 115-18	SAV-4	06C3069	Plagioclase	5.29 ± 0.21	99	0.060	0.51	9	5.35 ± 0.23	too radiogenic	too radiogenic	too radiogenic
Alia 115-26	SAV-5	06C3540	Groundmass	5.01 ± 0.04	100	1.000	1.61	21	5.02 ± 0.04	5.02 ± 0.04	290.1 ± 8.3	1.56
Alia 114-03	SAV-6	06C3569	Groundmass	4.24 ± 0.10	73	0.455	0.86	9	4.22 ± 0.09	too radiogenic	too radiogenic	too radiogenic
Alia 123-03	COM-1	06C2862	Groundmass	11.17 ± 0.17	78	0.290	2.59	16	11.09 ± 0.18	11.04 ± 0.24	301.6 ± 8.5	2.40
Alia 123-02	COM-2	07C2033	Groundmass	11.12 ± 0.13	48	0.360	4.46	5	11.03 ± 0.09	too radiogenic	too radiogenic	too radiogenic
Alia 124-11	BAY-1	07C1136	Groundmass	12.92 ± 0.12	76	0.234	1.96	16	12.87 ± 0.20	12.91 ± 0.14	298.8 ± 22.0	2.09
Alia 124-09	BAY-2	07C1627	Groundmass	12.77 ± 0.12	69	0.323	3.78	10	12.94 ± 0.13	too radiogenic	too radiogenic	too radiogenic
Alia 125-29	FAV-1	07C1203	Groundmass	12.94 ± 0.13	57	0.301	1.57	19	12.90 ± 0.13	12.96 ± 0.14	292.0 ± 9.2	1.60
Alia 125-04	FAV-2	07C1998	Groundmass	13.15 ± 0.16	35	0.223	2.83	6	12.79 ± 0.12	too radiogenic	too radiogenic	too radiogenic

[a]K/Ca values are calculated as weighted means for the age spectra. MSWD values for the age plateaus and inverse isochrons are calculated using N-1 and N-2 degrees of freedom, respectively. All samples from this study where monitored against FCT-3 biotite (28.03 ± 0.18 Ma) as calibrated by *Renne et al.* [1998]. Reported errors on the ^{40}Ar/^{39}Ar ages are on the 95% confidence level (2σ) including 0.3‰–0.4‰ standard deviation in the J value. All input parameters to the calculations are published in Table 2 of *Koppers et al.* [2003]. Due to the intensive acid leaching of the groundmass samples age dated, the atmospheric component (from alteration, absorption and trapped argon) in some cases may have been effectively removed, resulting in extremely high radiogenic components for the age plateaus and a clustering of the data points near the intercept on the ^{39}Ar/^{40}Ar axis. Whenever the radiogenic components for all steps included in the age calculations are higher than 95% we consider these data points "too radiogenic" to calculate meaningful isochrons.

submarine basalts, but a broad range of rock types: hawaiite, alkali basalt, trachybasalt, picrite basalt, mugearite, trachyte, phonolite, basanite and tephrite. Individual sample descriptions are presented in Appendix A. In this section, we will describe the $^{40}Ar/^{39}Ar$ analytical results (Figures 2 and 3 and Table 2) followed by the observed age systematics in the Samoan seamount trail.

[26] When analyzing groundmass samples, the $^{40}Ar/^{39}Ar$ incremental heating technique releases argon gas from different submicroscopic mineral phases at different heating steps because of their variable diffusive properties [e.g., *Koppers et al.*, 2000]. The advantage of this technique over a total fusion analysis is that alteration-derived argon can be identified and distinguished by the preferential release of the primary $^{40}Ar*$ and $^{39}Ar_K$ from different locations and mineral phases within the groundmass. These complex argon release histories of groundmass samples can be shown by plotting the age of individual heating steps against the cumulative percentage of $^{39}Ar_K$ released, whereby each "box" represents the relative size (horizontal) and 2σ analytical uncertainty (vertical) of each measured heating step (Figure 2). Within these age spectra, horizontal "age plateaus" containing at least 50% of the total $^{39}Ar_K$ released are believed to represent parts of these groundmasses that effectively remained closed since the time of crystallization (upon their eruption). Significant divergences to higher or lower ages, however, may result from a loss or gain of $^{40}Ar*$, the recoil of irradiation-derived $^{39}Ar_K$ and the preferential diffusive release of "discordant" argon components from alteration phases in the samples. In general, low-temperature heating steps release argon from sites that readily lose gas, such as the surface of a grain or very fine grained alteration minerals, whereas the high-temperature heating steps remove gas from more retentive sites, likely further within a mineral phase or from grains or minerals that will melt at higher temperatures.

[27] Groundmass samples were dated from Bayonaise, Combe, Favavesi, Manatu, Savai'i, Tamai'i, Tisa, Soso, Muli, between Tutuila and Tulaga, and Ofu. Their age plateaus comprise between 5 to 25 heating increments and range from 35% to 100% in the total amount of $^{39}Ar_K$ released. Only 2 out of the 26 groundmass experiments yielded plateaus less than 50% wide. In 46% of the cases concordance between the plateau, total fusion and isochron ages is observed, and 73% of the inverse isochron intercepts are within error of the 295.5 modern atmospheric ratio of $^{40}Ar/^{36}Ar$. For the remaining 6 ground-

masses no isochron could be calculated due to a larger than 95% yield in radiogenic argon (Table 2). All groundmass samples have high apparent ages at LT steps, with 83% also showing an increase in the K/Ca ratio. In contrast 66% of the groundmasses have low apparent ages at HT steps of which 91% show decreasing K/Ca values. In addition, the majority of the groundmass age spectra show exponential declines from the apparently "high age" LT steps to the age plateaus. In 25% of these cases the exponential declines seem to continue into the age plateaus, but with the distinction that, despite this mild sloping, all plateau steps are similar within 2σ uncertainty bounds. The age plateaus also show steady K/Ca ratios throughout the plateau, of which 41% have higher than bulk rock K/Ca values.

[28] The high apparent ages and increasing K/Ca ratios at LT heating increments most likely result from an alteration signature in the submarine basalts, whereas groundmass clinopyroxene and plagioclase tend to degas at high temperatures. The degassing of the latter minerals is often indicated by a sharp decrease in K/Ca and a rapid increase in $^{37}Ar_{Ca}$ [e.g., *Koppers et al.*, 2004], yet the outgassing of these Ca-rich (and very K-poor) minerals does not significantly contribute to the age plateaus. In addition, the very low temperature LT steps tend to have high $^{40}Ar_{atm}$ derived from high atmospheric components in the alteration phases, which all exponentially decline into the plateaus that typically are characterized by very high radiogenic $^{40}Ar*$ components. In some cases discordance between the total fusion and plateau ages indicates loss of $^{40}Ar*$ owing to submarine alteration, if the total fusion age is too low, or loss of $^{39}Ar_k$ by recoil, if the total fusion age is too high [*Koppers et al.*, 2000]. Nevertheless, most of the measured Samoan groundmass samples show concordances in these ages, indicating that their primary argon reservoirs were not significantly affected by alteration or recoil, and that these isotope systems have effectively remained closed. Overall, good reproducibility of the groundmass ages within one dredge haul and the close concordances of these groundmass ages with comagmatic mineral ages, show that performing high-resolution incremental heating age analyses on highly crystalline groundmass samples provide reliable estimates for the time of crystallization and eruption.

[29] Three biotite samples were dated from Tamai'i and Tulaga. These experiments resulted in 7 to 11 steps in the age plateaus, representing between 93% and 100% of the total amount of $^{39}Ar_K$ released. As the inverse isochron intercepts are

Geochemistry
Geophysics
Geosystems

G^3

KOPPERS ET AL.: EN ECHELON SAMOAN VOLCANIC TRAILS

10.1029/2010GC003438

within error of the modern atmospheric $^{40}Ar/^{36}Ar$ ratio, and as the plateau ages are concordant with their total fusion and isochron ages at the 95% confidence level, all quality criteria have been met. The high quality of these analyses are exemplified by reproducible ages between the ALIA D109-07 and D109-06 biotite experiments (0.88 ± 0.08 and 0.88 ± 0.05 Ma, respectively) and concordance with comagmatic K feldspar (0.83 ± 0.06 Ma) and groundmass (0.88 ± 0.08 Ma, inverse isochron) analyses.

[30] Five K feldspar samples were analyzed from Savai'i, Tamai'i and Tulaga. These samples meet the criteria for reliable age data, with all age plateaus comprising between 8 and 21 steps, and representing 77%–100% of the total amount of $^{39}Ar_K$ released. Again, there is concordance between the plateau and total fusion ages. Unfortunately, no inverse isochron intercepts were calculated as the data points in these plots are all clustered near the $^{39}Ar/^{40}Ar$ intercept, preventing the calculation of reasonable isochrons (Table 2). Typically, the reproducibility of the K feldspar experiments are good with identical ages between groundmass and K feldspar for ALIA-D111-07 (1.87 ± 0.03, 1.90 ± 0.03 Ma) and ALIA-D111-05 (1.93 ± 0.02, 1.92 ± 0.02 Ma).

[31] The only plagioclase sample is from Savai'i (ALIA D115-18) and yielded a reliable age. The plateau consists of 9 heating steps and represents 99% of the total amount of $^{39}Ar_K$ released. There is concordance between the plateau and total fusion ages, yet this age has a relatively large uncertainty at 5.29 ± 0.21 Ma, making it indistinguishable from the other ages that define a very narrow range between 4.98 and 5.06 Ma, but that have uncertainties of less than 0.04 Ma [Koppers et al., 2008].

5. Discussion

[32] Darwin [1851] noted that volcanic islands are often found in chains with active volcanism on one end and older coral atolls on the other. Accordingly, the western islands of Samoa have been described as appearing "younger" than the islands to the east based on the presence of large volumes of very recent (posterosional) volcanism [e.g., Dana, 1849]. To explain this "reversed" age progression from west to east, some researchers attributed the origin of Samoa to volcanism induced by cracks in the Pacific Plate and related this to the complex tectonic setting close to the Tonga subduction zone [Hawkins and Natland, 1975; Natland, 1980; Natland and Turner, 1985]. Menard [1986, p. 187] surmised, however, that Samoa is a remarkable "example of rejuvenated volcanism superimposed on shield-building [lavas] generated by a hotspot." Recent geochemical, geochronological and tomography data have now provided unequivocal support for a hot spot origin of the Samoa seamount trail [Hart et al., 2004; Montelli et al., 2004; Workman et al., 2004; Koppers et al., 2008]. Intraplate volcanism in Samoa is thus more complex compared to other seamount trails and it is likely that its evolution is determined by a combination of processes, either acting sequentially or synchronously. In this discussion we address the origin of the 15 Myr age progression observed in Samoa, comparing it to existing GPS velocity models and Absolute Plate Motion (APM) models for the Pacific Plate. We also discuss the significance of the en echelon subtracks characterizing the morphology of the post-1.5 Ma Eastern Samoan volcanic province (ESAM), the late stage posterosional volcanism on Samoa, and implications for intraplate volcanism in general.

5.1. Samoan Age Progression and the Hot Spot Model

[33] A hot spot origin for the Samoan archipelago would require a mantle plume located in eastern Samoa that has been constantly producing magma over the last 15 Myr, and perhaps longer, if the 23.9 Ma Alexa seamount is included as part of the hot spot trail [Hart et al., 2004]. The involvement of a mantle plume in Samoa would therefore be evidenced by a linear trail of volcanoes increasing in age to the west, starting from the currently active Vailulu'u seamount, and recording a rate and direction proportional to the rate and direction of the Pacific Plate over the last 15 Myr. Our new age data, together with previously published age data, imply such a linear age progression for the initial shield-building volcanics of the Samoan islands and seamounts. Focusing on just submarine samples (orange circles and brown squares in Figure 4) we find that the age data have a calculated linear age progression of ~7.6 cm/yr with Vailulu'u as the "zero-aged" hot spot and a precisely defined 5.02 ± 0.03 Ma (n = 5) tie point at Savai'i located 380 km west of the hot spot [Koppers et al., 2008]. The distribution of all Samoan seamount ages show that their upper bounds, representing the earliest stages of the seamount construction, as expected, fall on or closely below the age progression line. Because seamounts have their own internal magmatic systems, with sometimes extensive rift
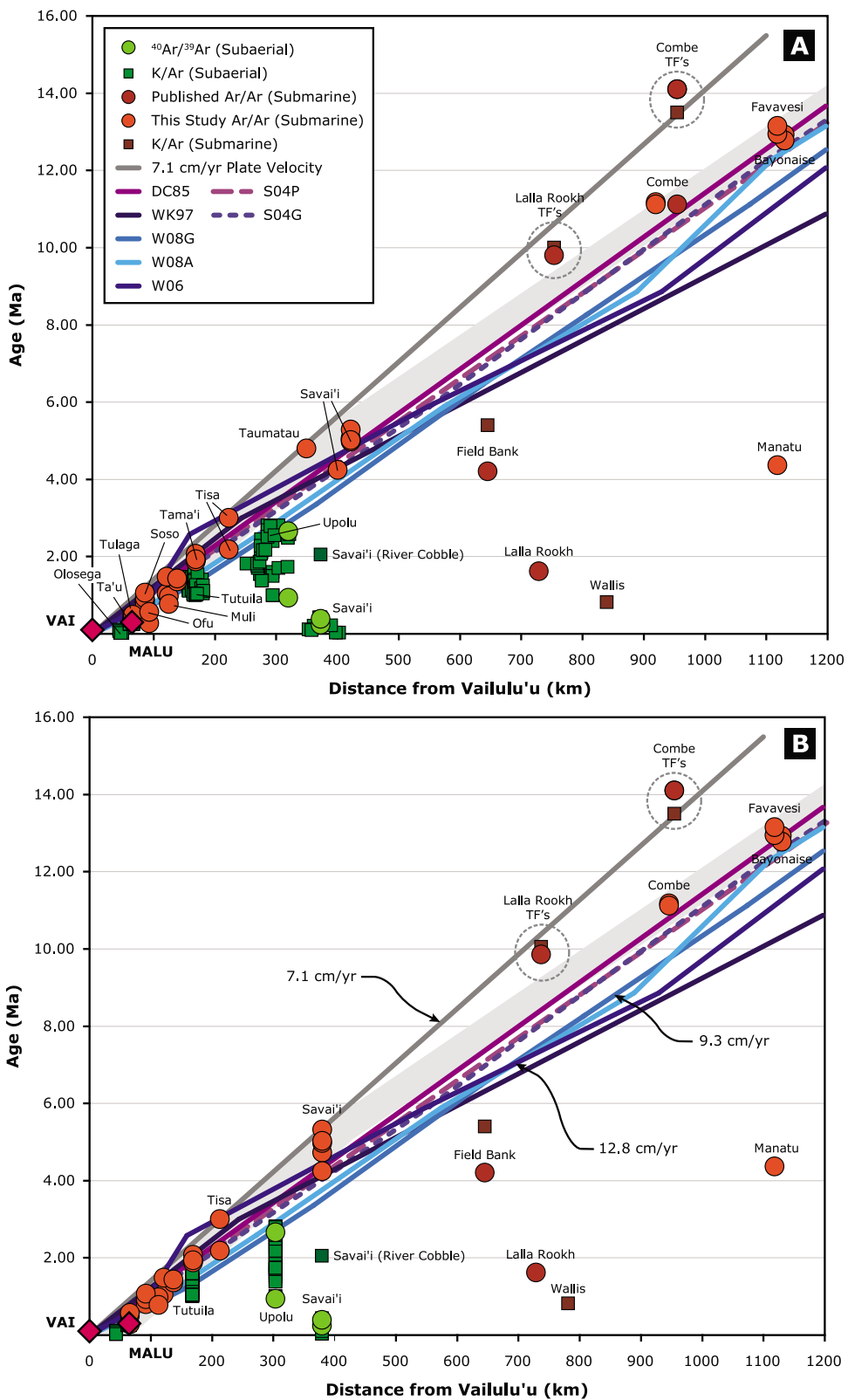
Figure 4

systems, dredge locations may not accurately define the location of the Samoan hot spot at the time of eruption. Therefore, the age systematics described above come even more into focus when we plot the same age data with respect to the "centers" of the volcanic islands and seamounts (Figures 4b and 5b).

[34] One plate motion model used for comparison is the constant 7.1 cm/yr plate velocity derived from an average of present-day velocities at nearby GPS stations [*Hart et al.*, 2004]. This is very close to the 6.9 cm/yr plate velocity as predicted by the REVEL and NUVEL-1A-NNR models, which use geodetic data and relative plate motions (mainly based on spreading rates and transform fault orientations), respectively, to aid in reconstructing absolute plate motions by assuming there is a no net rotation (NNR) of the lithosphere [*DeMets et al.*, 1994; *Sella et al.*, 2002; *Ruellan et al.*, 2003; *Hart et al.*, 2004]. Another category of Absolute Plate Motion (APM) models provides rotational poles for several time intervals (e.g., 0–0.78, 0.78–2.58, 2.58–5.89, 5.89–8.86 and 8.86–12.29 Ma) as derived by inverting the orientation, morphology and ages of Pacific seamount trails *other* than Samoa [e.g., *Wessel et al.*, 2006; *Wessel and Kroenke*, 2008]. The W06 and W08G are two models that solely use the location of seamounts in multiple seamount trails with respect to their active hot spot locations to obtain the best possible geometric fit for the plate rotation poles, whereas the W08A model also uses seamount age information in the fitting procedure. These latter APM models all assume a long-term fixed reference frame of hot spots in the Earth's mantle, and although the REVEL and NUVEL-1A-NNR models provide comparable estimates for absolute plate motion, these motions are relative to different reference frames. It has been shown that the Pacific Plate moves 20%–30% faster relative to hot spots than its calculated motion in the NNR reference frame [e.g., *Argus and Gordon*, 1991].

[35] These different types of APM models thus provide an independent means of testing the observed Samoan age progression as measured by K/Ar and ^{40}Ar/^{39}Ar geochronology. As can be seen in Figures 4 and 5, our ^{40}Ar/^{39}Ar age data best approaches the 7.1 cm/yr constant plate motion model (gray line), yet the ages show significant differences with respect to the most recent fixed hot spot APM models [*Wessel and Kroenke*, 1997; *Wessel et al.*, 2006; *Wessel and Kroenke*, 2008]. First, the majority of the new ages for seamounts younger than 5 Ma are up to 0.9–1.3 Myr older than predictions from the W08A and W08G models [*Wessel and Kroenke*, 2008] that assume a fixed reference frame of deep mantle plumes. Second, the differences are more obvious when comparing the age progression with the "average" Pacific Plate age progression predicted by the W08A model, which at 9.3 cm/yr is about 2.2 cm/yr faster than observed in Samoa. Even though this APM model has been optimized to best fit available seamount ages, the W08A model still carries a large uncertainty in the time interval 0–5 Ma, translating into a total range of possible age progressions between 8.1 and 12.8 cm/yr (gray band in Figure 6). As a result, the ~7.6 cm/yr age progression recorded for Samoa over the last 5 Myr barely overlaps with the W08A model, and we argue here that the relatively large uncertainties in this W08A or any other APM model are masking the true diversity of the age progressions observed in individual seamount trails across the Pacific. In fact, seamount trails formed on the Pacific Plate are producing separate data arrays with significantly different angles in a plot of seamount age versus plate motion opening angle (e.g., compare Samoa and Hawaii in Figure 6). This spread is not due to (analytical) scatter in the age data but a function of different geological processes underlying the formation of these seamount trails. It is unclear, however, what processes can cause the

Figure 4. Age versus distance plots for the Samoan seamount trail comparing subaerial versus submarine samples against a constant 7.1 cm/yr GPS plate speed and recent APM models. (a) Overall age systematics for the WESAM and ESAM volcanic provinces since 16 Ma using actual sample/dredge locations. (b) Same plot but using the midpoint location for each seamount or volcanic center instead. In these plots the constant 7.1 cm/yr REVEL and NUVEL-1A-NNR plate velocity model is shown as a gray line, and the Absolute Plate Motion (APM) models assuming fixed hot spots (*Duncan and Clague* [1985], DC85; *Wessel and Kroenke* [1997], WK97; *Wessel et al.* [2006], W06; *Wessel and Kroenke* [2008], W08G and W08A) are shown as blue lines. In addition, two APM models allowing for hot spot motions are included, assuming motion of the Hawaiian hot spot in the Pacific alone and assuming motion of four hot spots (Hawaii, Louisville, Reunion, and Walvis) globally and transferred to the Pacific Plate through the global plate circuit (*Steinberger et al.* [2004], S04P and S04G). The best fit age progressions based on our seamount age record is indicated by the shaded gray area, allowing for ~1 Myr shield building durations and preferentially fitting the oldest observed ages. Vailulu'u is taken as the "zero age" volcano in this hot spot trail. All great circle distances (in km) have been calculated with respect to a common point located in Savai'i (far away and west from the en echelon trails) and then renormalized so that Vailulu'u becomes the "zero point" along the distance axis.
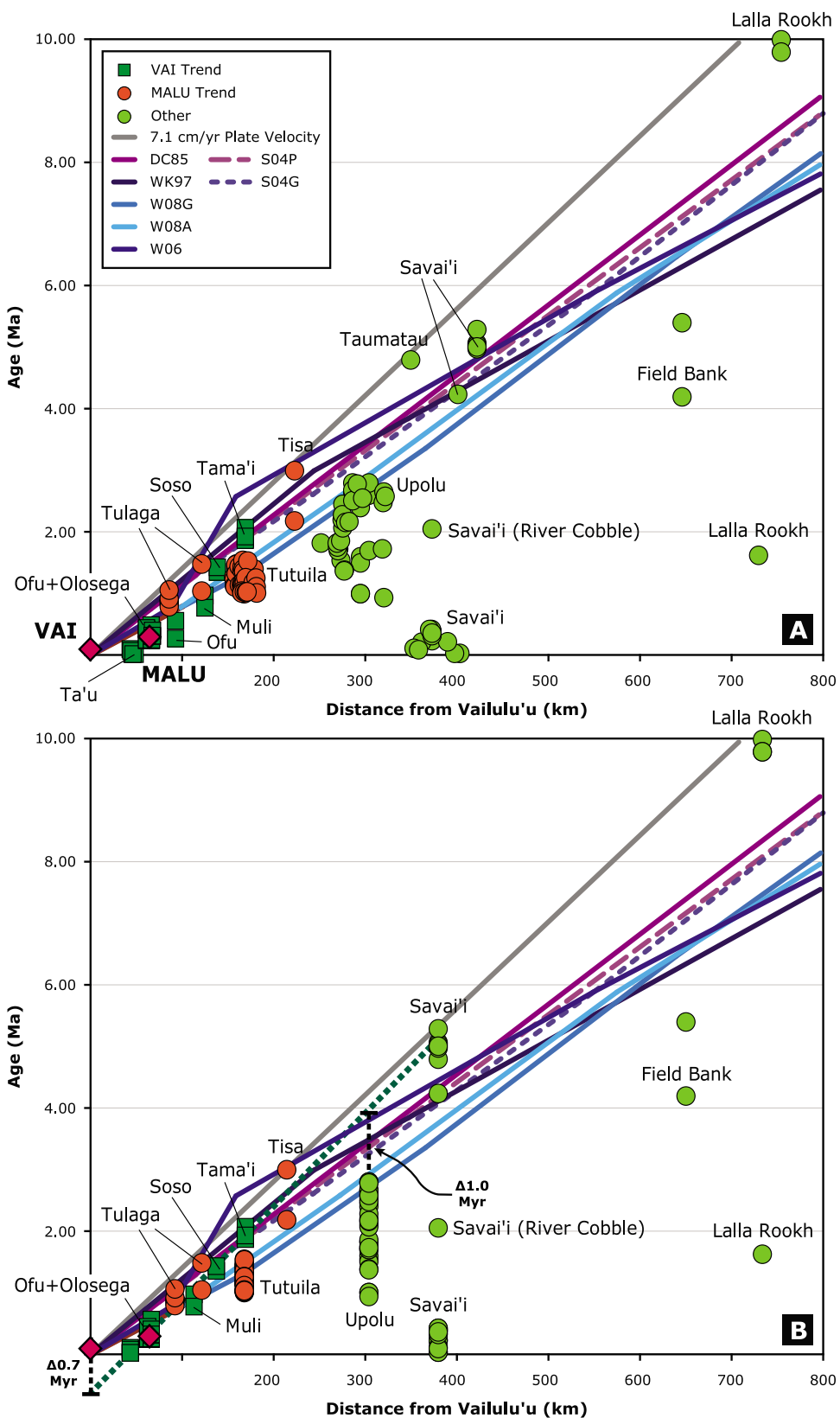
Figure 5

differences between the observed disparate age progressions. From the standpoint of hot spot fixity, having seamount trails recording different age progressions in the same time interval and on the same lithospheric plate is problematic, because it means that at the largest scale the Pacific Plate is not behaving rigidly and that local plate velocities vary significantly from the "average" plate motion. The solution is not straightforward, but it is to be expected that secondary processes or inter–hot spot motions need to be invoked to systematically offset these age progressions, so that they can record apparently faster or slower plate motions compared to the "average" APM model predictions.

[36] For Samoa our observations show that both the GPS plate motion model and the observed $^{40}Ar/^{39}Ar$ age progression point toward a significantly slower "apparent" plate motion over the last 5 Myr (Figure 6). The question now arises what could cause such an apparently slow age progression for Samoa? It likely is not caused by the motion of the Samoan plume predicted by *Hart et al.* [2004] as their modeled plume motion would be in a southeastern direction, opposite to the northwestern Pacific Plate motion and causing an apparent *increase* in the observed age progression. Even if the Samoan plume is being blown to the northeast by the mantle wind escaping from under the rolling back Pacific Plate, this would be more or less orthogonal to the northwestern plate direction and thus would not significantly affect the Samoan age progression. However, these mantle flow models are sensitive to uncertain parameters such as the plume initiation age and viscosity structure of the mantle in that part of the Pacific domain. It is conceivable that a change in these model assumptions could alter the outcome of these predictions for Samoa, but that remains to be tested. From Figure 6 it is clear that both Samoa and Cobb have the slowest recorded age progressions and both are close to a subduction zone. All other seamount trails (except maybe for Caroline) are much more removed from a convergent plate

boundary. These more intraplate hot spot systems therefore may have been less impeded by the interaction with other plates, allowing for faster local plate velocities that are more consistent with the expected plate rotation models. This is unlikely as it implies that the Pacific Plate is not rigid throughout. Alternatively, we could argue that Samoa has been recording an age progression closer to the "true" Pacific Plate velocity and that all other seamount trails in the Pacific (such as Hawaii) have been recording age progressions that are apparently faster. Looking at mantle flow models for the Pacific mantle domain and predicted plume motions [*Steinberger et al.*, 2004; *Steinberger and Antretter*, 2006], it seems that the Hawaiian plume moved N160°E over the last 5 Myr and consequently it had a component of plume motion opposite the northwestern plate motion. This makes it is possible that Hawaii has recorded a combined motion of its plume and the Pacific Plate, resulting in an faster age progression relative to all other seamount trails in the Pacific. It is intriguing that the Samoan age progression for the last 5 Myr also is slower than the predictions from APM models taking into account plume motions. In Figure 4 and 5 we have plotted the age progressions as predicted from two such models: One accommodates the 15° southern motion of the Hawaiian hot spot between 80 and 50 Ma (S04-P [*Koppers et al.*, 2004; *Steinberger et al.*, 2004; *Steinberger and Gaina*, 2007]) and the other accommodates plume motions of four global hot spots (i.e., Hawaii, Louisville, Reunion and Walvis) that have been transferred via the global plate circuit to the Pacific Plate (S04-G [*Koppers et al.*, 2004; *Steinberger et al.*, 2004; *Torsvik et al.*, 2008]). However, since plume motions were more prevalent during the Late Paleocene and the Cretaceous, these model predictions do not deviate much from the fixed hot spot models after 50 Ma, and both the S04-P and S04-G models follow the *Duncan and Clague* [1985] model (DC85) closely between 0 and 16 Ma (Figure 4). It remains unexplained

Figure 5. Age versus distance plots for the Samoan seamount trail comparing the VAI and MALU subtracks against a constant 7.1 cm/yr GPS plate speed and recent APM models. (a) Blowup for last 10 Myr with the VAI and MALU trends separated and using actual sample/dredge locations. (b) Same plot but using the midpoint location for each seamount or volcanic center. Note the 0.5–0.7 Myr offset of Vailulu'u from the VAI trend and that placing Vailulu'u below the horizontal axis (and thus into the future) would improve the overall fit to the 7.1 cm/yr GPS plate speed model considerably. Also note the ~0.5 Myr and ~1.0 Myr age gaps for Tutuila and Upolu volcanics, respectively, which indicate that for these Samoan islands the entire range of shield-building volcanics has not been sampled yet. Finally, note that there are no K/Ar or $^{40}Ar/^{39}Ar$ age dates of the posterosional lavas from Upolu or Tutuila, yet the major Salani, Mulifanua, and Lefaga formations on Upolu and the Leone formation on Tutuila appear to be postglacial and thus similar in age to the K/Ar-dated posterosional volcanics of Savai'i Island that are younger than 0.22 Ma [*McDougall*, 2010]. See Figure 4 for notations and methods used.
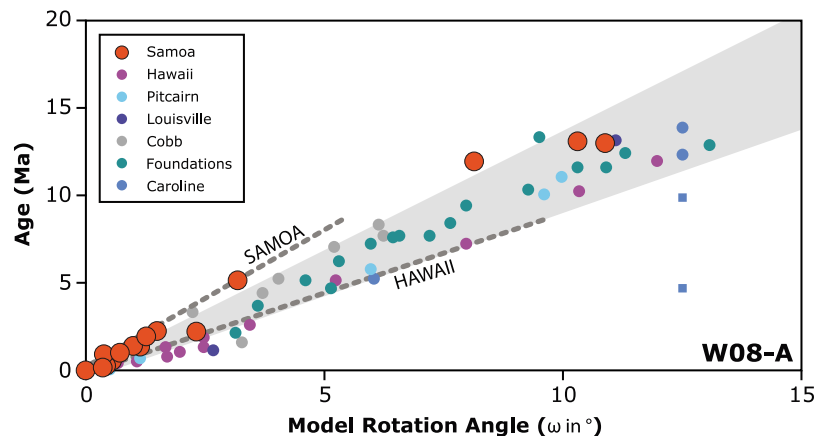
Figure 6. Seamount ages versus opening angle of the Pacific Plate based on the W08A APM model of *Wessel and Kroenke* [2008]. By plotting the seamount ages against opening angle (and *not* great circle distance) with respect to their active hot spot location, we can compare all age progressions from seamount trails on the Pacific Plate. In the context of fixed hot spots, plate tectonic theory mandates that all age progressions should be similar within uncertainty limits, assuming a rigid lithospheric plate and a constant angular plate velocity. In this plot this means that all seamount trails should produce data arrays that overlap and that have similar slopes, which is not the case. Two dashed lines are indicated to show the significant difference in angle and thus age progression between Samoa and Hawaii.

what caused the apparent slower plate motion for the Samoan part of the Pacific Plate and why all other Pacific seamount trails and most APM models record a faster age progression up to 30%–40%.

[37] Prior to 5 Ma the 7.1 cm/yr model does not hold and the age progression seems to shift to a faster apparent plate motion up to ~9–13 cm/yr (Figure 4). When looking at this older segment in Samoa, we have to ignore an age determination from sample 7–11 of Combe Bank that actually would fit the 7.1 cm/yr age progression [*Hart et al.*, 2004], but gave an older (inaccurate) total fusion age of 14.1 ± 2.2 Ma [*Duncan*, 1985]. As we have no incremental heating age spectra for this sample at hand, and as this sample was *not* acid treated to remove alteration, we prefer to use the more precise plateau age of sample 7–100 at 11.12 ± 0.12 Ma [*Hart et al.*, 2004] instead, which we have reproduced in two different ALIA dredge samples with ages of 11.12 ± 0.13 and 11.17 ± 0.17 Ma (Table 2). The 9.8 Ma tie point at Lalla Rookh [*Duncan*, 1985] is also a $^{40}Ar/^{39}Ar$ total fusion age of a sample *not* treated by acid leaching and therefore for the same reasons may be of lesser quality. Ignoring the 14.1 Ma Combe and 9.8 Ma Lalla Rookh ages in our calculations, we obtain a high-quality regression line through the precise Savai'i tie point at 5.0 Ma, the 11.1 Ma age of Combe, and our new Favavesi and Bayonaise $^{40}Ar/^{39}Ar$ ages, ranging in age between 12.8 and 13.2 Ma. This translates into an age progression of

~9.4 cm/yr between 5 and 13 Ma and thus is much closer to what is predicted by the fixed hot spot APM models (Figure 4b).

5.2. En Echelon Trails of the Eastern Samoa Volcanic Province

[38] At a smaller scale, the age systematics are further complicated by the existence of two en echelon lineaments in the ESAM that both were volcanically active between approximately 1.5 Ma and the present day. When the age results are separated into the VAI and MALU subtracks on the age-distance plots, they form two linear arrays that significantly overlap with matching westward increases in seamount age (Figure 5). Consequently, extended periods of concurrent volcanism occurred in both subtracks. For example, Soso and Tutuila had periods of overlapping volcanism, as well as Tamai'i and Tisa, whereas volcanism on Muli was concurrent with volcanism on both Tulaga and the elongated rift zone between Tutuila and Tulaga. Concurrent volcanism also existed between the youngest volcanoes in these subtracks, with active or historic volcanism occurring at Vailulu'u and Malumalu [*Staudigel et al.*, 2006; *Sims et al.*, 2008]. Interestingly, the age progression delineated by the VAI subtrack does not connect with Vailulu'u in the age-distance plots, as the measured ages of this "zero-aged" submarine volcano plot ~0.5–0.7 Myr above the best fit line interpolated to the (negative) vertical axis (Figure 5b). A first explanation may be that Vailulu'u

itself is not part of the VAI trend and represents a singular seamount starting its own en echelon subtrack [*Hart et al.*, 2004]. A more likely explanation may be that all samples age dated in the VAI trend are consistently sampling a time later in their shield-building stages, while Vailulu'u represents a shield volcano not even *halfway* through the same volcanic stage. This latter scenario could explain the ~0.5–0.7 Myr age difference, in particular as shield-building may take about ~1 Myr until completion and Vailulu'u appears to be not older than a few hundred thousand years, and 7 of 9 analyzed samples are less than 8 kyr [*Sims et al.*, 2008]. Moreover, placing Vailulu'u at minus 0.7 Ma in the age-distance plots (i.e., at a future later stage in its volcanic evolution) considerably improves the overall fit to the 7.1 cm/yr constant plate motion model.

[39] Based on their ^{40}Ar/^{39}Ar geochronology the VAI and MALU subtracks can thus be attributed to the same hot spot. However, from a morphological point of view it is clear that both subtracks must have formed independently from two different eruption sites (Figure 7). Close inspection of Figure 7a reveals that seamounts in each subtrack are dominated by subparallel N110°E rift zones, are interconnected at their bases, and originated from two isolated locations offset by ~69 km (i.e., the measured distance between Vailulu'u and Malumalu). In the VAI subtrack Muli, Ofu, Olosega, Ta'u and Vailulu'u delineate a more or less continuous ridge of seamounts and volcanic islands. Tamai'i and Soso deviate slightly northward from this trend and they do not connect to each other or to Muli seamount. In fact, the morphology of Soso seamount is dominated by a major N30°E rift zone that may be the extension of the NNE secondary rift zone protruding from Tutuila Island. In the MALU subtrack Malumalu and Tulaga are directly connected to the ESE rift zone extending from Tutuila Island. When the age progressions are viewed in map view (Figure 7b), the independent nature of both subtracks becomes even more evident, as the Samoan volcanoes are systematically aging toward the west and quite likewise along both en echelon lineaments.

[40] This map view also shows that during the time period that Tutuila Island was forming from 1.5 to 1.0 Ma, the Samoan hot spot trail started to bifurcate, morphing from a robust singular trail of seamounts and volcanic islands into two separate en echelon subtracks. Tutuila is unique because it is a large volcanic complex (with a volume of ~5,000 km^3, Earthref.org, 2010) and because of its primary N70°E rift zone that is markedly different from the N110°E oriented VAI and MALU subtracks

(Figure 7a). *Walker and Eyre* [1995] take note of this in their study of dike systems on the island. Interestingly, Tutuila also has a secondary N30°E rift zone that extends toward Soso seamount in the VAI trend, which has an age of 1.3–1.5 Ma concurrent with volcanism on Tutuila (Figure 7b). On the other hand, Soso and Tamai'i seamount, are relatively small seamounts with respective volumes of ~60 and ~230 km^3 (Earthref.org, 2010) and are morphologically different from other VAI seamounts. They are located off axis from the VAI trend, are characterized by basal depths (~4,800 m) much deeper than those of the other en echelon seamounts and demonstrate highly undeveloped morphologies (i.e., characterized by a low number of rift zones). Soso is unique in that it shows a clear structural relationship with the northeastern secondary rift extending from Tutuila. Tamai'i exhibits no such relationship. However, as it is located only 60 km north of Tutuila, and as there are many smaller volcanic cones in the intervening space, it is possible that Tamai'i is a satellite of the Tutuila rift system as well. This is countered by higher ^{206}Pb/^{204}Pb isotopic signatures for Soso and Tamai'i (Figures 8 and 9), making them (slightly) different from seamounts in the VAI and MALU subtracks, from Tutuila Island, and from typical posterosional volcanism occurring widespread through Samoa. Nonetheless, the isotopic signatures of Soso and Tamai'i are most similar to islands and seamounts from the VAI trend, and may represent a new extreme composition for the VAI-type volcanoes.

[41] Observed differences in isotope geochemistry between the VAI and MALU subtracks provide another line of evidence pointing to two eruption sites originating from within a single mantle plume. The Hawaiian Loa and Kea trends are a good analog that, for example, can be explained by a model of a mantle plume of a single composition matrix containing streaks of another composition [*Ren et al.*, 2005]. In such a model, the different locations of the multiple eruption sites would allow for a preferential sampling of either the matrix, a more exotic streak in the Samoan mantle plume, or a combination of both. In the plot of delta ^{208}Pb/^{204}Pb versus ^{87}Sr/^{86}Sr, shield-building lavas of the MALU trend volcanoes (dark green symbols) span a much larger region in both isotopic dimensions, whereas the VAI trend shield volcanoes (red symbols) occupy a narrower isotopic space and at a markedly lower ^{87}Sr/^{86}Sr ratio (Figure 8a). These systematics are evident for ^{143}Nd/^{144}Nd ratios as well, where MALU volcanoes have lower values for any given ^{208}Pb/^{204}Pb ratio (Figure 8b), and in lead isotopic

Figure 7

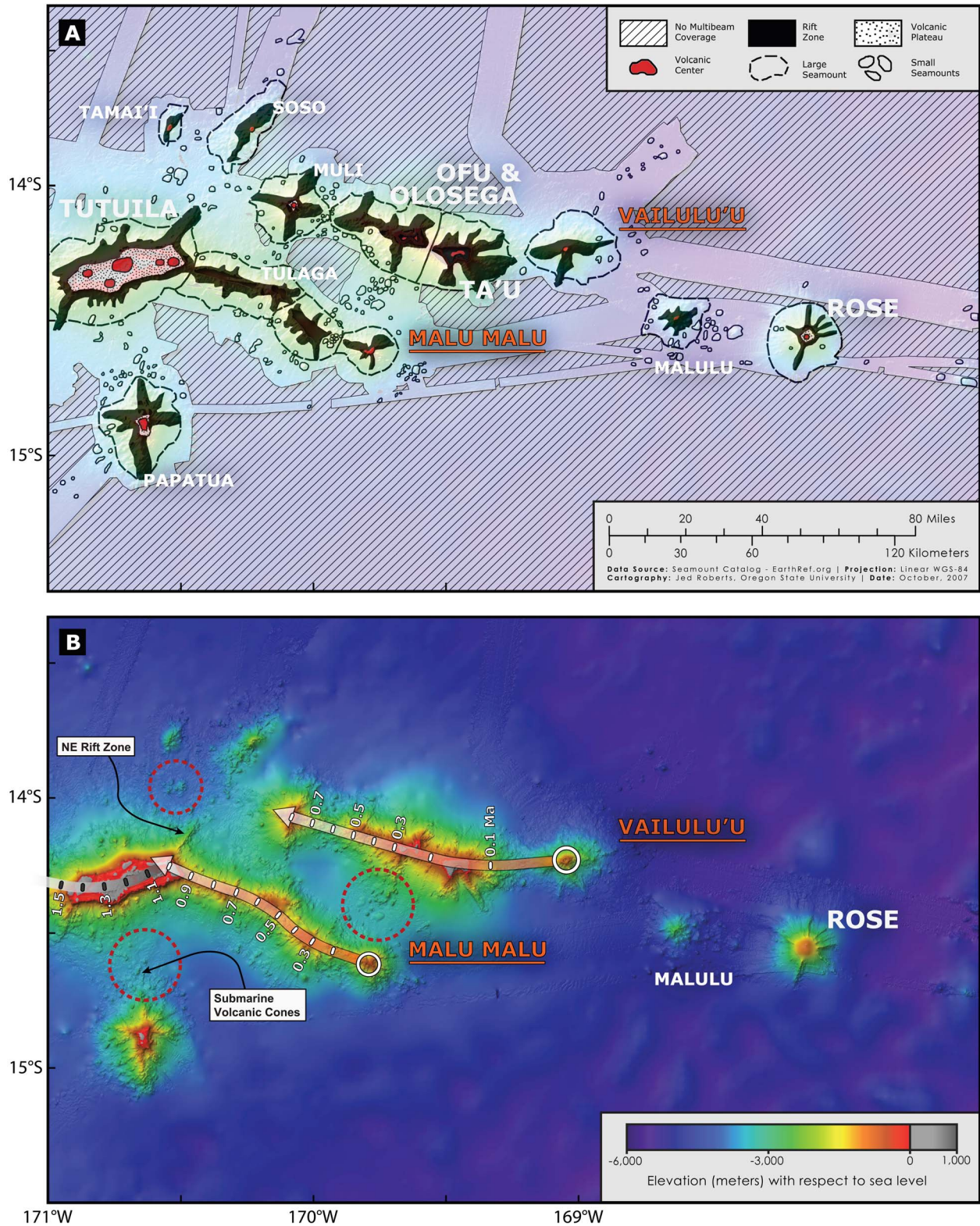space $^{207}Pb/^{204}Pb$ and $^{208}Pb/^{204}Pb$ (not shown) are consistently higher at any given $^{206}Pb/^{204}Pb$ ratio (Figure 8c). Analogous to the Loa-Kea model for Hawaii, this may suggest a MALU composition plume with VAI composition streaks, or vice versa, or as both trends overlap on the "depleted" end and point toward FOZO [*Hart et al.*, 1992; *Jackson et al.*, 2007b], it may be easier to imagine FOZO being the "matrix" with two different "EM2 streaks." In this we ignore extreme $^{87}Sr/^{86}Sr$ and $^{143}Nd/^{144}Nd$ signatures observed in the deep submarine shield basalts from Savai'i Island [*Jackson et al.*, 2007a]. These extreme Savai'i shield basalts are even more unlike the VAI trend volcanoes and thus exaggerate the differences in isotopic source composition. Though basalts from Upolu plot within the MALU array for $^{208}Pb/^{204}Pb$, $^{207}Pb/^{204}Pb$, $^{87}Sr/^{86}Sr$ and $^{143}Nd/^{144}Nd$ ratios, in terms of $^{206}Pb/^{204}Pb$ ratios they are distinctly lower. This may indicate that Upolu lavas have sampled a mantle source similar to the one feeding posterosional volcanism that in Samoa is characterized by $^{206}Pb/^{204}Pb$ ratios lower than 18.9 [e.g., *Workman et al.*, 2004; *Koppers et al.*, 2008].

[42] Shield-building basalts in the ESAM also decrease in $^{206}Pb/^{204}Pb$ with distance from the hot spot (Figure 9). In the reverse sense, this means that the MALU and VAI subtracks are becoming more enriched while younging, a trend that seems to extend all the way from older seamounts in the WESAM volcanic province. There are however some exceptions. Soso, Tamai'i, Tisa, Lalla Rookh and Fa'avevesi are all plotting above this Pb age evolutionary trend, suggesting they may have been sourced in a different part of the Samoan plume. As indicated above, Upolu is lower in $^{206}Pb/^{204}Pb$ and falls below the Pb age trend, which provides evidence for mixing toward postshield and posterosional compositions. This observation is apparent from the age progressions as well, whereby Upolu appears to be ~1.0 Myr younger than suggested by other shield volcanoes (Figure 5b). Correcting for this age gap and mapping Upolu onto the $^{206}Pb/^{204}Pb$ age trend for Samoan volcanoes, it is expected that Upolu shield lavas formed around 3.6 Ma with $^{206}Pb/^{204}Pb$ ratios of ~19, comparable to shield ratios in Savai'i.

[43] In summary, all Samoan seamounts studied (except Manatu) show the same EM2 geochemical pedigree, and their overall trend and age progression are in good alignment with GPS plate motion models. However, when focusing on detailed age systematics and differences in isotope composition, a single hot spot "eruption site" in the Samoan region fails to explain the concurrent volcanism seen throughout the younger than 1.5 Ma end of the chain. A single mantle plume with two distinct eruption sites, one located near Vailulu'u and another in the vicinity of Malumalu, both tapping slightly different sources from different zones within a single mantle plume may better explain the concurrent volcanism in these two subtracks. The en echelon MALU and VAI trends for that reason merely seem to be the products of short length-scale processes internal to the larger Samoan mantle plume that have been active only over relatively short geological time scales.

5.3. Deviations From the Hot Spot Model and Alternative Interpretations

[44] In the light of our $^{40}Ar/^{39}Ar$ age results for submarine basalts, it is becoming obvious that the subaerial ages measured for several of the Samoan islands represent anomalously young and late stage volcanism [*Duncan*, 1985; *Hart et al.*, 2004; *McDougall*, 2010]. Every land sample from Savai'i is posterosional with the possible exception of a ~2 Ma trachytic river cobble (from a low-quality total fusion $^{40}Ar/^{39}Ar$ age) that may be late shield stage material [*Workman et al.*, 2004]. Even though this river cobble is considerably older than the posterosional volcanics (typically all younger than 0.4 Ma), it is still several million years younger than the $^{40}Ar/^{39}Ar$ age for onset of Savai'i shield volcanism around 5.0 Ma [*Koppers et al.*, 2008]. Similar

Figure 7. (a) Geomorphological interpretation of major volcanic structures in the ESAM volcanic province with 200 m multibeam bathymetry in background. Note that most seamounts in the VAI and MALU trends are interconnected by N110°E rift zones. Vailulu'u itself is somewhat offset to the northeast with respect to the VAI trend but has a western rift zone connecting to Ta'u Island. However, both Tamai'i and Soso are morphologically different from the other VAI seamounts because they are not dominated by a major N110°E rift zone. They instead exhibit a single N30°E rift zone and appear offset to the north and thus off axis from the overall VAI trend. Tutuila is structurally atypical as well, having a N70°E orientation and showing a major N30°E rift zone that seems to extend into Soso seamount in the VAI trend. Also interesting are small (unsampled) seamounts that possibly represent a group of late stage or posterosional underwater volcanic cones, occurring all across the ESAM region. (b) Measured ages for the VAI and MALU trends on an interpretative map with 200 m bathymetric grid in foreground and predicted bathymetry from 1 km satellite altimetry from *Smith and Sandwell* [1997] in the background. Ages in the age trends are tick marked every 0.1 Myr.
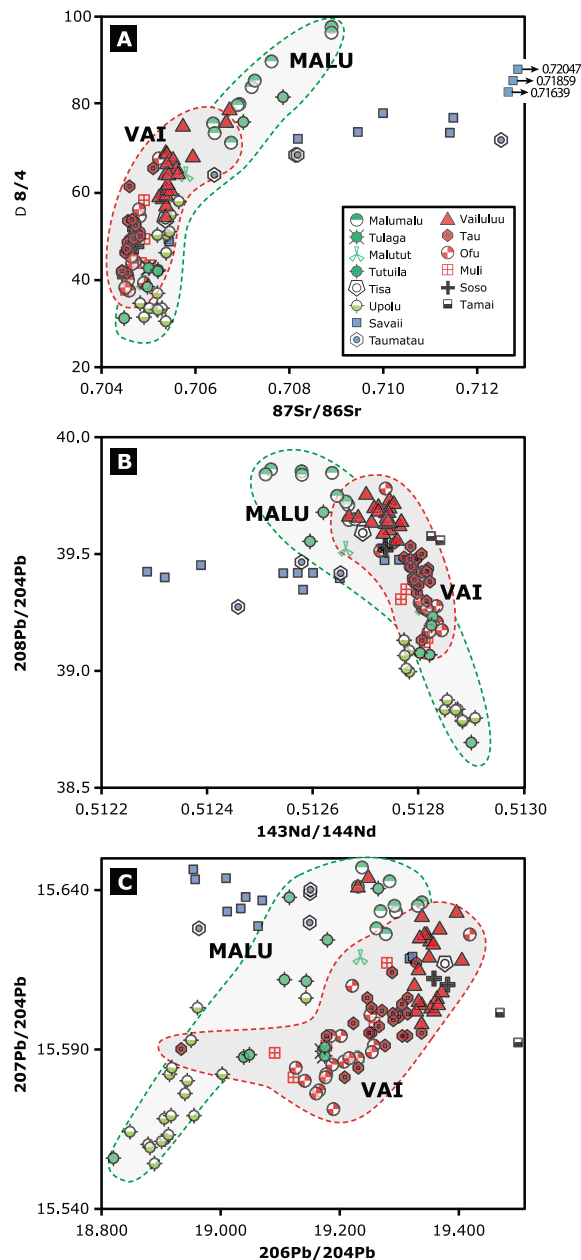
Figure 8. Isotope systematics in the Samoa seamount trail for the VAI (red) and MALU (dark green) trends. Only shield-building stage basalts are plotted and seamounts not readily identified as VAI or MALU trend are indicated in separate colors, such as Savai'i (blue), Upolu (light green), and Soso and Tamai'i (black). (a) Delta ^{208}Pb/^{204}Pb versus ^{87}Sr/^{86}Sr. (b) ^{207}Pb/^{204}Pb versus ^{206}Pb/^{204}Pb. (c) ^{208}Pb/^{204}Pb versus ^{143}Nd/^{144}Nd. Data compiled from *Workman et al.* [2004], *Jackson et al.* [2007a, 2007b], *Workman et al.* [2006, 2008], and *Jackson et al.* [2010].

observations can be made for Upolu and Tutuila, with subaerial sample ages plotting more than 1.0 and 0.5 Myr below the 7.1 cm/yr age progression found in the submarine samples (Figure 5b). Other

notable deviations from these age progressions are the young ages of Lalla Rookh, Wallis and Manatu. One sample from Wallis reported by *Duncan* [1985] likely represents a posterosional lava flow and one dredge sample from Savai'i reported by *Jackson et al.* [2010] were also rejuvenated, as do two of
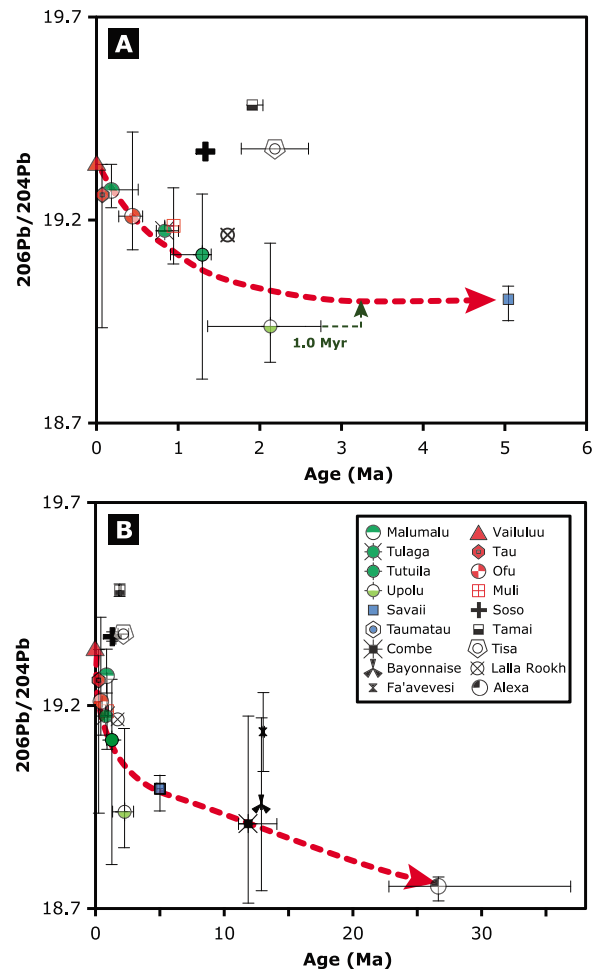
Figure 9. (a) ^{206}Pb/^{204}Pb versus age systematics in the Samoa seamount trail for the VAI (red) and MALU (dark green) trends. Basalts from Savai'i and Upolu Island are shown by blue and light green symbols; all other ESAM and WESAM seamounts are indicated by black and white symbols. Only shield-building stage basalts are plotted, and we only display data pairs for samples with both age and isotope data. The only exceptions are Upolu and Ta'u, for which the plotted data reflect separate sample sets. (b) All data since 37 Ma. From Figure 5b it appears that Upolu is ~1.0 Myr too young compared to the overall Samoan age progression. Extrapolating this offset (toward a higher age) on the ^{206}Pb/^{204}Pb age curve (red arrow) predicts a shield-building ^{206}Pb/^{204}Pb ratio of ~19 for Upolu, similar to Savai'i's shield signature [*Koppers et al.*, 2008]. Same data sources as in Figure 8 combined with our new ^{40}Ar/^{39}Ar ages and data from *Hart et al.* [2004].

the three samples from Lalla Rookh [*Duncan*, 1985; *Hart et al.*, 2004], and a sample from Field [*Duncan*, 1985].

[45] The interesting fact is that posterosional volcanism is occurring more or less synchronously across Savai'i, Upolu and Tutuila, but most of these eruptions only occurred since ~0.4 Ma. This recent Samoan-wide phase of posterosional volcanism seems to be structurally controlled, as late stage volcanic cones and lava flows are all centered along a rift zone that continues from island to island. Detailed multibeam mapping reveals a couple of extensive fields with dozens of small-scale features, which could be interpreted as late stage volcanic cones scattered in between larger seamounts and volcanic islands (Figure 7b). These features are most prevalent throughout the ESAM from Ofu-Olosega westward, on the northern flank of Papatua, and stretching south from Ofu and Olosega to the Tulaga and Malumalu. At this point, constraining their origin is a speculative exercise, and they may turn out to be debris from large mass wasting events as well, often seen on the flanks of the Hawaiian Islands [e.g., *Presley et al.*, 1997]. It will be an important future research task to map out these posterosional products over time, on land and below the sea surface, and in terms of their isotope geochemistry, so that we can discern when this posterosional volcanism started and how far away the islands were with respect to the northern most terminus of the Tonga Trench at that initiation time.

[46] Several mechanisms associated with shallow lithospheric magma production may be responsible for these kinds of intraplate volcanism not directly related to mantle plumes, which may have formed the rejuvenated volcanoes throughout the Samoa region. These mechanisms include mantle "hot lines," crack propagation, self-perpetuating volcanic chains, reactivated plate boundaries, incipient plate boundaries, membrane and extensional stresses, gravitational anchors, reheated slabs, buoyant decompression melting of mantle heterogeneities, dike propagation, meteorite impacts, and leaky transform faults and rifting unrelated to uplift [*Shaw and Jackson*, 1973; *Oxburgh and Turcotte*, 1974; *Jackson and Shaw*, 1975; *Jackson et al.*, 1975; *Bonatti and Harrison*, 1976; *Shaw et al.*, 1980; *Clague and Dalrymple*, 1987; *Clague et al.*, 1989; *Anderson*, 1998; *Czamanske et al.*, 1998; *Hieronymus and Bercovici*, 1999; *Beutel et al.*, 2005; *Elkins-Tanton and Hager*, 2005; *Clouard and Gerbault*, 2008]. It is inconceivable to assume that rigid tectonic plates moving around and colliding on a spherical Earth would not become

stressed in certain locations, and since it requires less energy to penetrate a preexisting weakness in the lithosphere than to create an entirely new plate boundary [*Gurnis et al.*, 2000], extensional volcanism would likely focus around these stress cracks [*Natland and Winterer*, 2005]. These notions support the idea that certain places in a tectonic plate are predisposed to having a volcanic feature, even if they are located in the middle of a more or less rigid plate. An example of this is the reconditioning of oceanic lithosphere by the emplacement of earlier seamounts trails [*Staudigel et al.*, 1991; *Jackson et al.*, 2010] producing a likely place for the plate to crack and initiate new eruptions [*Koppers and Staudigel*, 2005]. Contraction of the oceanic lithosphere due to its cooling over time may also explain lithospheric cracks. When new oceanic crust is created at spreading centers it is warmer relative to older crust and as the crust cools it warps and cracks may form [*Wright et al.*, 2002; *Sandwell and Fialko*, 2004]. This lithospheric-cooling-induced cracking of a plate may be responsible for the formation of volcanic ridges in the Pacific Ocean such as Pukapuka Chain [*Sandwell and Fialko*, 2004]. "Crack spots" are a type of extensional volcanism resulting from preconditioned cracks in the lithosphere weakened even further by plate stress [*Wessel and Kroenke*, 2000]. Once the lithosphere is cracked, magma generation works in a "top-down" way, allowing for the passive upwelling of more fertile upper mantle material, which subsequently may result in the production of low-volume decompression melts [*Anderson*, 2001; *Foulger and Natland*, 2003]. However, because of the repeated passage of the Samoan region over different hot spot systems (i.e., four times over the last 40 Myr) it is more likely that the underlying asthenosphere has been depleted of fertile mantle and has become more viscous over time. This would make it more unlikely for "crack-induced extension" to have sampled fertile mantle in the shallow asthenosphere, as that kind of mantle material must now be sampled from below this "refractory keel" or be replenished by a deeper-seated Samoan mantle plume [*Jackson et al.*, 2010].

[47] Despite the lack of a suitably fertile source in the shallow mantle beneath Samoa, stress buildup close to a plate boundary undoubtedly will lead to complexities in the formation of nearby seamounts trails. In the case of Samoa, late stage posterosional volcanism can be understood if we consider the generation of local lithospheric stresses in the Pacific Plate, where it subducts and deforms close to the NE terminus of the Tonga Trench. Some researchers claim that this model could explain the entire volcanic

history of the Samoan trail, arguing that melting originated near the base of the lithosphere from the accumulation of stresses with the Pacific Plate bending upon its descent into the trench [*Hawkins and Natland*, 1975; *Natland and Winterer*, 2005]. We argue here that this bending may indeed have put some extra stress on the Pacific Plate, but only causing recent extension (or failure) that may have opened up pathways for the surge of posterosional volcanism since 0.4 Ma. However, in prior times, before 5.0 Ma, it seems unlikely that these stresses influenced the formation of the Samoan volcanoes as plate reconstructions place the Samoan hot spot at a significant (>1,500 km) distance from the NET [*Koppers et al.*, 2008].

5.4. Prolonged Volcanism

[48] Though shield-building volcanism represents only a small portion of the entire eruption history of a volcano, it can still span several hundred thousand to a few million years, depending mainly on the speed and thickness (or age) of the overlying tectonic plate. The Hawaiian shield-building phase typically lasts 0.5–1.5 Myr [*Clague et al.*, 1989] and based on the slower predicted plate velocities [*Wessel et al.*, 2006] for Samoa over most of the past 12 million years, such durations should be considered a minimum for Samoan volcanoes. The Cook Islands, which are another seamount trail located relatively nearby in the Pacific Ocean, have experienced shield durations up to 4 Myr [*Turner and Jarrard*, 1982] showing the potential for even longer durations of shield building in Samoa. Therefore, extended periods of shield building are a reasonable explanation for the fact that many of the measured ages for submarine sampled Samoan lavas are younger than the predicted model ages by up to 1.3 Myr for the 7.1 cm/yr model, because the oldest material may have been completely covered by younger shield lava and was unattainable for dredging and age dating. Data from subaerial lavas on Upolu indicate a measured duration lasting 1.9 Myr (Figure 5a). If we would extend this duration to 2.9–3.3 Myr, the origination of volcanism on Upolu would correspond very well with the predicted ages from the 7.1 cm/yr model (Figure 5b). Since *all* age-dated samples from Upolu were collected subaerially, it is realistic to assume that older shield volcanism may be found on the outer submarine flanks of the island (unfortunately these were not targeted for dredging during the ALIA expedition). Savai'i Island is comparable to Upolu in size and may have experienced a similar lengthy shield

building phase. Assuming that the 2 Ma river cobble [*Workman et al.*, 2004] is in fact representative of late shield building stage at Savai'i, the duration of shield volcanism would be 3.2 Myr, which is comparable to the 3.3 Myr upper limit of the hypothesized shield duration of Upolu. Tutuila has evidence of a shield duration of 0.5 Myr [*Mcdougall*, 1985; *Natland and Turner*, 1985], but there likely is a sampling bias since all age dated samples were collected subaerially on this island as well. And perhaps, if its lower submarine flanks were to be dredged in the future, earlier shield lavas may be recovered.

5.5. Implications for Intraplate Volcanism

[49] Long-lived plume tails imaged using mantle tomography techniques seem to have diameters only between 100 and 400 km [*Montelli et al.*, 2004]. S wave velocity anomaly patterns characterizing the mantle beneath Hawaii show evidence for warmer temperature regions more than 400 km wide at shallow 100–400 km depths, and 100–200 km wide up to 1,500 km depth [*Wolfe et al.*, 2009]. The zone of influence of an impinging mantle plume on an overriding tectonic plate is thus relatively wide, and maybe wider than previously assumed, although the actual melting zone (i.e., where temperatures are above the solidus) is likely less wide. As a result, hot spot volcanism may form seamounts with significant variations in source chemistry perpendicular to (and along) the track of a seamount trail, maybe as much as 200 km in each direction and concurrently. The VAI and MALU subtracks are spaced only ~50 km apart and fall within this potential zone of influence. This means that at such a short length scale processes occurring within the Samoan plume itself, and variations in composition within its plume conduit, will have a direct effect on the formation of this seamount trail. In addition, it is also likely to experience local effects of deformation and stress in the plate on the formation of the Samoan seamount trail, from the impingement of the plume itself on the Pacific Plate and the loading by individual seamounts. The subparallel ridges of the Hawaii-Emperor seamount trail are a good example [*Jackson and Shaw*, 1975; *Jackson et al.*, 1975], as are the Loa and Kea geochemical trends in the Hawaiian Ridge [*Staudigel et al.*, 1984; *Ren et al.*, 2005] which are spaced only 39 km apart. The VAI and MALU trends might share a similar origin to the Hawaiian subtracks, explaining the slight oblique offset of these subtracks from the overall seamount trail orientation, their somewhat different age progressions

from the overall 7.1 cm/yr Samoan age progression, and their difference in isotopic signature.

6. Summary

[50] Most previous samples from Samoa were collected on its volcanic islands, inadvertently biasing the sampling toward relatively young subaerial lava flows, primarily representing posterosional volcanism or the final products of their waning shield-building stages. In this study, we show that sampling deep on the submarine flanks yields older shield volcanics that give better age estimates for the beginning construction of the Samoan seamounts and islands. This has considerably simplified the age versus distance systematics along the Samoan seamount trail, allowing us to directly compare our age data to existing (independent) models for the absolute motion of the Pacific Plate. It has also allowed us to look at small-scale phenomena associated with Samoa's intraplate volcanism, as expressed in two en echelon subtracks, the VAI and MALU trends, defining the morphology of the ESAM volcanic province since 1.5 Ma.

[51] Based on the available K/Ar and $^{40}Ar/^{39}Ar$ age data, including our new submarine age determinations, we find a general increase in age moving west from Vailulu'u. This age progression in the Samoan seamount trail is roughly linear, if focusing on the ages of shield (and submarine) samples only. Even though the Samoan seamount trail changes in its morphology from a robust singular seamount trail into the VAI and MALU subtracks, the linear age progression remains intact. Between 0 and 5 Ma the age progression is closest to fitting a constant 7.1 cm/yr plate motion, analogous to current GPS measurements for the Pacific plate in this region. Between 5 and 13 Ma the older seamounts (and only including the latest $^{40}Ar/^{39}Ar$ ages) record an apparently faster plate motion of ~9.4 cm/yr. Most interestingly, all $^{40}Ar/^{39}Ar$ ages lie above the "average" age progression predicted by modern APM models, based on assuming fixed hot spots or moving hot spots alike, and the Samoa age progression itself is systematically different from age progressions in other seamount trails in the Pacific. Taken at face value, this suggests that in the region of Samoa the Pacific Plate apparently moved slower than in the rest of the Pacific, which is an unlikely scenario in plate tectonics. An alternative model is that over the last 5 Myr these other hot spot systems experienced a component of plume motion opposite to the northwestern motion of the Pacific Plate. The N160°E Hawaii plume motion over the last 5 Myr

predicted from mantle flow modeling is consistent with this model and would generate apparently faster age progression for Hawaii compared to Samoa.

[52] The VAI and MALU trends volcanoes also can be distinguished by their differences in isotope geochemistry. Although the overall EM2 pedigree remains prevalent in all samples dredged and analyzed so far, minor variations between the VAI and MALU trends point to a sampling of different zones internal to the Samoan plume conduit or a different "mix" of components in the same mantle plume source. There also are variations evident with geological time. Shield-building basalts increase in $^{206}Pb/^{204}Pb$ along both the MALU and VAI subtracks, which means that their seamounts are becoming more enriched while maturing, a trend that seems to extend all the way from older seamounts in the WESAM volcanic province.

[53] Finally, it is becoming evident that a typical Samoan volcano may have a prolonged volcanic history, spanning up to 3 or 5 Myr. Even though hot spot–driven intraplate volcanism seems the central cause for producing the most voluminous and deepest parts of the Samoan seamounts and islands, the bending of the downgoing plate around the northeastern termination point of the Tonga Trench may have put extra stress on the Pacific Plate. In turn, this may have caused recent extension (or failure) in the Pacific Plate that may have opened up pathways for the surge of Samoan posterosional volcanism, resurfacing (part of) the islands of Savai'i, Upolu and Tutuila since 0.4 Ma. This late stage volcanism is evident not only in the resurfacing of the islands of Samoa, but also in the occurrence of many small volcanic cones on the submarine flanks of large seamounts and islands. The relatively high volume of the posterosional volcanics, compared to the same late stage volcanism in Hawaii, would require an unusual fertile mantle source beneath Samoa. It also could be explained by a focusing of partial melts being squeezed from in between the downgoing slab and a viscous "keel" attached to the bottom of the Samoan lithosphere [*Jackson et al.*, 2010]. In the latter case the posterosional lavas are expected to inherit the strong EM2 pedigree from the Samoan mantle plume, the common geochemical signature seen in the shield-building lavas throughout the ESAM and WESAM volcanic provinces.

Appendix A: Sample Descriptions

[54] Figure A1 contains a short sample description of all basalts used for age dating. The dredge
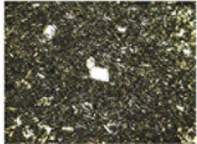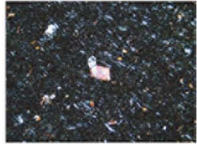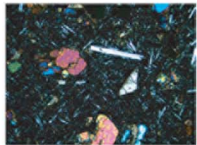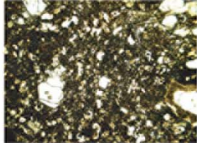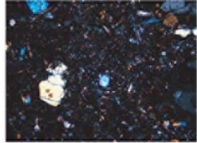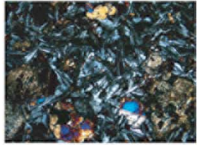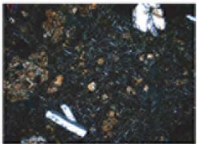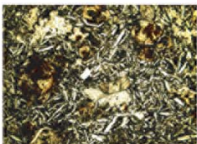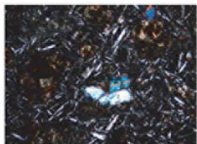
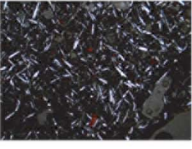| ALIA Dredge	Thin Section Photograph		Description	Material(s) Analyzed
	Plain Polarized Light	Cross Polarized Light		
Combe Bank 123-03			Non-vesicular basalt; **phenoxx** = 2% cpx, >1% plg, >1% olivine; **grndm** = hypocrystalline with 45% plg; **alt** = 5% in groundmass, olivine is altered; **other** = Mn crust	Groundmass Leached*, handpicked 109.6 mg
Savai'I Island 115-03			Vesicular (1%) alkalic trachybasalt; **phenoxx** = 25% cpx, 10% plg; **grndm** = hypocrystalline with 60% plg, 10% cpx; **alt** = 10% in groundmass	Groundmass Leached*, handpicked 112.3 mg
128-21			Vesicular (40%) alkali basalt; **phenoxx** = 25% cpx; **grndm** = hypocrystalline with 20% cpx, 10% plg; **alt** = 20% in groundmass	Groundmass Magnet, leached*, handpicked 103.9 mg

ALIA Dredge	Thin Section Photograph		Description	Material(s) Analyzed
	Plain Polarized Light	Cross Polarized Light		
Savai'I Island 115-28			Vesicular (5%) hawaiite; **phenoxx** = 5% cpx; **grndm** = holocrystalline with 90% plg and kfs; **alt** = 5% in groundmass	Groundmass Magnet, leached*, handpicked 111.1 mg K-Feldspar Magnet, leached#, handpicked 64.3 mg
115-18			Vesicular (20%) trachybasalt; **phenoxx** = 5% plg, 3% cpx; **grndm** = holocrystalline with 20% plg; **alt** = 10% in groundmass; **other** = thin Mn crust	K-Feldspar Magnet, leached#, handpicked 30.9 mg
115-26			Vesicular (5%) trachyandesite; **phenoxx** = 5% plg, 3% cpx, <1% olivine; **grndm** = holocrystalline with 95% plg and 5% cpx; **alt** = 3% in phenocrysts, 1% in groundmass	Groundmass Magnet, leached*, handpicked 103.9 mg

Figure A1.   Sample descriptions of all basalts used for age dating.
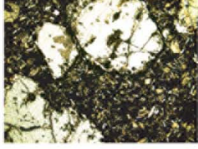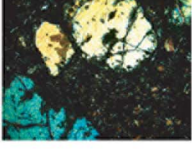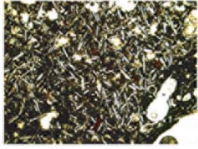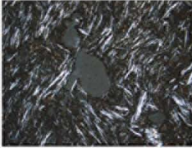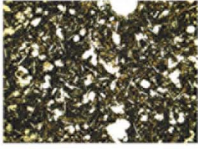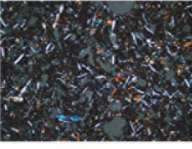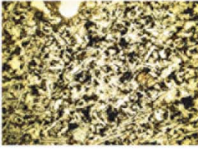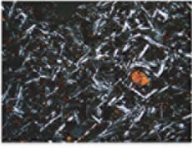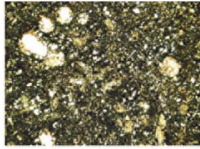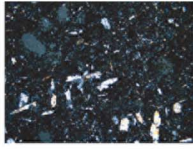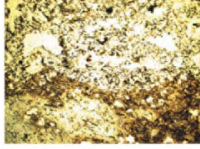
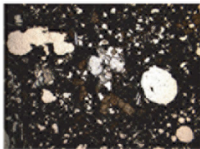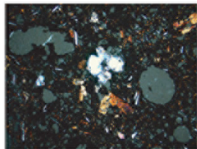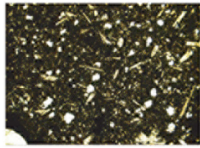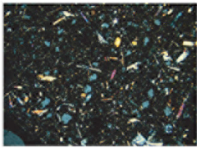| ALIA Dredge	Thin Section Photograph		Description	Material(s) Analyzed
	Plain Polarized Light	Cross Polarized Light		
Savai'I Island 114-03			Non-vesicular picrite basalt; **phenoxx** = 20% cpx, 5% olivine; **grndm** = hypocrystalline with 40% plg; **alt** = all of olivine, 5% in groundmass, 2% in cpx; **other** = thin Mn crust	Groundmass Leached* (2X), magnet handpicked 109.6 mg
Tisa Seamount 113-21			Vesicular (15%) mugearite; **phenoxx** = n/a; **grndm** = hypocrystalline with 45% plg; **alt** = 3% in groundmass; **other** = thick Mn crust	Groundmass Leached*, handpicked 129.1 mg
Tama'i Seamount 111-07			Vesicular (3%) trachyte; **phenoxx** = <1% cpx, <1% plg; **grndm** = holocrystalline with 95% plg and kfs; **alt** = minor; **other** = thin Mn crust	Groundmass magnet, leached*, handpicked 117.9 mg

ALIA Dredge	Thin Section Photograph		Description	Material(s) Analyzed
	Plain Polarized Light	Cross Polarized Light		
Tama'i Seamount 111-05			Vesicular (5%) trachyte; **phenoxx** = <1% biotite; **grndm** = holocrystalline plg,kfs; **alt** = minor	K-Feldspar magnet, leached#, handpicked 35.7 mg Biotite magnet, rinsed, handpicked 10.6 mg
Soso Seamount 110-21			Vesicular (20%) basalt; **phenoxx** = n/a; **grndm** = hypocrystalline with 20% plg, 15% cpx; **alt** = 15% in groundmass	Groundmass Leached*, handpicked 106.2 mg
Rift between Tutuila and Tulaga 108-01			Vesicular (5%) basanite/tephrite; **phenoxx** = 3% cpx; **grndm** = holocrystalline plg; **alt** = 7% in groundmass, 3% in vesicles, 1% in phenocrysts	Groundmass Leached*, handpicked 102.3 mg

Figure A1.   (continued)

ALIA Dredge	Thin Section Photograph		Description	Material(s) Analyzed
	Plain Polarized Light	Cross Polarized Light		
Muli Seamount				
104-09			Vesicular (5%) basalt; **phenoxx** = 3% plg; **grndm** = hypocrystalline with 10% cpx, 5% plg; **alt** = 3% in groundmass, alteration in vesicles	Groundmass Leached*, handpicked 111.5 mg
Tulaga Seamount				
109-07			Vesicular (7%) phonolite; **phenoxx** = 1% plg, kfs <1% biotite; **grndm** = holocrystalline with 90% plg and kfs; **alt** = 7% in groundmass	K-Feldspar magnet, leached#, handpicked 29.8mg Biotite magnet, rinsed, handpicked 6.6 mg
109-06			Vesicular (5%) phonolite; **phenoxx** = 1% plg, kfs, 1% cpx, <1% biotite; **grndm** = holocrystalline plg, kfs; **alt** = 10% in phenocrysts, 5% in groundmass	K-Feldspar magnet, leached#, handpicked 34.0 mg Biotite magnet, rinsed, handpicked 10.0mg

ALIA Dredge	Thin Section Photograph		Description	Material(s) Analyzed
	Plain Polarized Light	Cross Polarized Light		
Ofu Island				
103-04			Vesicular (20%) basanite/tephrite; **phenoxx** = 5% cpx, <1% olivine; **grndm** = hypocrystalline with 30% cpx, 2 % plg; **alt** = 5% in groundmass, all olivine; **other** = thin Mn crust	Groundmass Leached*, handpicked 104.5 mg
107-09			Vesicular (10%) basanite/tephrite; **phenoxx** = 7% plg, 5% cpx; **grndm** = hypocrystalline with 10% plg, 5% cpx; **alt** = 20% in phenocrysts, 10% in groundmass.	Groundmass Leached*, handpicked 108.1 mg

Phenoxx = phenocrysts
Grndm = groundmass, plg = plagioclase, kfs = K-feldspar and cpx = clinopyroxene
Alt = alteration

*Grndm leaching   - 1 hour in 1N HCl, 1 hour in 6N HCl, 1 hour in 1N HNO3 and 1 hour in ultra pure deionized water
#Feldspar leaching - 1 hour in 1N HCl, 1 hour in 6N HCl, 1 hour in 1N HNO3, 15 minutes 5% HF,
        30 mintes 1N HNO3 and 1 hour in ultra pure deionized water

Figure A1.   (continued)

number, location and two thin section photographs (one in plain and one in crossed polarized light) representative of the rock sample are given as well. In the fifth column the product used for age dating is listed, including the sample weight of the hand-picked groundmass or mineral separates.

Acknowledgments

References

Abouchami, W., A. W. Hofmann, S. J. G. Galer, F. A. Frey, J. Eisele, and M. Felgenson (2005), Lead isotopes reveal bilateral asymmetry and vertical continuity in the Hawaiian mantle plume, *Nature*, *434*(7035), 851–856, doi:10.1038/nature03402.

Anderson, D. L. (1998), The scales of mantle convection, *Tectonophysics*, *284*(1–2), 1–17, doi:10.1016/S0040-1951(97)00169-8.

Anderson, D. L. (2001), Top-down tectonics?, *Science*, *293*, 2016–2018, doi:10.1126/science.1065448.

Argus, D. F., and R. G. Gordon (1991), No-net-rotation model of current plate velocities incorporating plate motion model Nuvel-1, *Geophys. Res. Lett.*, *18*(11), 2039–2042, doi:10.1029/91GL01532.

Beavan, J., P. Tregoning, M. Bevis, T. Kato, and C. Meertens (2002), Motion and rigidity of the Pacific Plate and implications for plate boundary deformation, *J. Geophys. Res.*, *107*(B10), 2261, doi:10.1029/2001JB000282.

Beutel, E. K., S. Nomade, A. K. Fronabarger, and P. R. Renne (2005), Pangea's complex breakup: A new rapidly changing stress field model, *Earth Planet. Sci. Lett.*, *236*(1–2), 471–485, doi:10.1016/j.epsl.2005.03.021.

Bonatti, E., and C. G. A. Harrison (1976), Hot lines in the Earth's mantle, *Nature*, *263*, 402–404, doi:10.1038/263402a0.

Campbell, I. H., and R. W. Griffiths (1990), Implications of mantle plume structure for the evolution of flood basalts, *Earth Planet. Sci. Lett.*, *99*, 79–93, doi:10.1016/0012-821X(90)90072-6.

Clague, D. A., and G. B. Dalrymple (1987), The Hawaiian-Emperor volcanic chain part I. Geologic evolution, *U.S. Geol. Surv. Prof. Pap.*, *1350*, 5–54.

Clague, D. A., G. B. Dalrymple, T. L. Wright, F. W. Klein, R. Y. Koyanagi, R. W. Decker, and D. M. Thomas (1989), The Hawaiian-Emperor chain, in *The Geology of North America*, vol. N, *The Eastern Pacific Ocean and Hawaii*, edited by E. L. Winterer, D. M. Hussong, and R. W. Decker, pp. 187–287, Geol. Soc. of Am., Boulder, Colo.

Clouard, V., and M. Gerbault (2008), Break-up spots: Could the Pacific open as a consequence of plate kinematics?, *Earth Planet. Sci. Lett.*, *265*(1–2), 195–208, doi:10.1016/j.epsl.2007.10.013.

Courtillot, V., A. Davaille, J. Besse, and J. Stock (2003), Three distinct types of hotspots in the Earth's mantle, *Earth Planet. Sci. Lett.*, *205*(3–4), 295–308, doi:10.1016/S0012-821X(02)01048-8.

Czamanske, G. K., A. B. Gurevitch, V. Fedorenko, and O. Simonov (1998), Demise of the Siberian plume: Paleogeographic and paleotectonic reconstruction from the prevolcanic and volcanic record, north-central Siberia, *Int. Geol. Rev.*, *40*(2), 95–115, doi:10.1080/00206819809465200.

Dalrymple, G. B., and D. A. Clague (1976), Age of the Hawaiian-Emperor bend, *Earth Planet. Sci. Lett.*, *31*, 313–329, doi:10.1016/0012-821X(76)90113-8.

Dana, J. D. (1849), *Geology. United States Exploring Expedition (With Atlas). C. Wilkes*, Putnam, New York.

Darwin, C. (1851), *Geological Observations on Coral Reefs*, Volcanic Islands, and on South America, Smith, Elder and Co., London.

Davies, D. R., and J. H. Davies (2009), Thermally driven mantle plumes reconcile multiple hot-spot observations, *Earth Planet. Sci. Lett.*, *278*(1–2), 50–54, doi:10.1016/j.epsl.2008.11.027.

Davis, A. S., M. S. Pringle, L. B. G. Pickthorn, D. A. Clague, and W. C. Schwab (1989), Petrology and age of alkalic lava from the Ratak Chain of the Marshall Islands, *J. Geophys. Res.*, *94*(B5), 5757–5774, doi:10.1029/JB094iB05p05757.

DeMets, C., R. G. Gordon, D. F. Argus, and S. Stein (1994), Effect of recent revisions to the geomagnetic reversal time scale on estimates of current plate motions, *Geophys. Res. Lett.*, *21*(20), 2191–2194, doi:10.1029/94GL02118.

Duncan, R. A. (1985), Radiometric ages from volcanic rocks along the New Hebrides–Samoa Lineament, in *Geological Investigations of the Northern Melanesian Borderland*, vol. 3, edited by T. M. Brocker, pp. 65–74, Circum.-Pac. Counc. for Energy and Miner. Resour., Houston, Tex.

Duncan, R. A., and D. A. Clague (1985), Pacific plate motion recorded by linear volcanic chains, in *The Ocean Basins and Margins*, vol. 7A, *The Pacific Ocean*, edited by A. E. A. Nairn, F. L. Stehli, and S. Uyeda, pp. 89–121, Plenum, New York.

Elkins-Tanton, L. T., and B. H. Hager (2005), Giant meteoroid impacts can cause volcanism, *Earth Planet. Sci. Lett.*, *239*(3–4), 219–232, doi:10.1016/j.epsl.2005.07.029.

Fleck, R. J., J. F. Sutter, and D. H. Elliot (1977), Interpretation of discordant ^{40}Ar/^{39}Ar age-spectra of Mesozoic tholeiites from Antarctica, *Geochim. Cosmochim. Acta*, *41*, 15–32, doi:10.1016/0016-7037(77)90184-3.

Foulger, G. R., and J. H. Natland (2003), Is "hotspot" volcanism a consequence of plate tectonics?, *Science*, *300*(5621), 921–922, doi:10.1126/science.1083376.

Govers, R., and M. J. R. Wortel (2005), Lithosphere tearing at STEP faults: Response to edges of subduction zones, *Earth Planet. Sci. Lett.*, *236*(1–2), 505–523, doi:10.1016/j.epsl.2005.03.022.

Gurnis, M., S. Zhong, and J. Toth (2000), On the competing roles of fault reactivation and brittle failure in generating plate tectonics from mantle convection, in *The History and Dynamics of Global Plate Motions*, *Geophys. Monogr. Ser.*, vol. 121, edited by M. A. Richards, R. G. Gordon, and R. D. Van der Hilst, pp. 73–94, AGU, Washington, D. C.

Hart, S. R. (1969), K, Rb, Cs contents and K/Rb, K/Cs ratios of fresh and altered submarine basalts, *Earth Planet. Sci. Lett.*, *6*(4), 295–303, doi:10.1016/0012-821X(69)90171-X.

Hart, S. R., E. H. Hauri, L. A. Oschmann, and J. A. Whitehead (1992), Mantle plumes and entrainment: Isotopic evidence, *Science*, 256(5056), 517–520, doi:10.1126/science.256.5056.517.

Hart, S. R., et al. (2000), Vailulu'u undersea volcano: The new Samoa, *Geochem. Geophys. Geosyst.*, (1), 1056, di:10.1029/2000GC000108.

Hart, S. R., M. Coetzee, R. K. Workman, J. Blusztajn, K. T. M. Johnson, J. M. Sinton, B. Steinberger, and J. W. Hawkins (2004), Genesis of the Western Samoa seamount province: Age, geochemical fingerprint and tectonics, *Earth Planet. Sci. Lett.*, 227(1–2), 37–56, doi:10.1016/j.epsl.2004.08.005.

Hawkins, J. W., and J. H. Natland (1975), Nephelinites and basanites of the Samoan linear volcanic chain: Their possible tectonic significance, *Earth Planet. Sci. Lett.*, 24, 427–439, doi:10.1016/0012-821X(75)90150-8.

Hieronymus, C. F., and D. Bercovici (1999), Discrete alternating hotspot islands formed by interaction of magma transport and lithospheric flexure, *Nature*, 397(6720), 604–607, doi:10.1038/17584.

Huneke, J. C. (1976), Diffusion artifacts in dating by stepwise thermal release of rare gases, *Earth Planet. Sci. Lett.*, 28, 407–417, doi:10.1016/0012-821X(76)90202-8.

Huneke, J. C., and S. P. Smith (1976), The realities of recoil: ^{39}Ar recoil out of small grains and anomalous age patterns in ^{39}Ar-^{40}Ar dating, *Proc. Lunar Sci. Conf.*, 7th, 1987–2008.

Jackson, E. D., and H. R. Shaw (1975), Stress fields in central portions of Pacific Plate: Delineated in time by linear volcanic chains, *J. Geophys. Res.*, 80(14), 1861–1874, doi:10.1029/JB080i014p01861.

Jackson, E. D., E. A. Silver, and G. B. Dalrymple (1972), Hawaiian-Emperor chain and its relation to Cenozoic circumpacific tectonics, *Geol. Soc. Am. Bull.*, 83, 601–618, doi:10.1130/0016-7606(1972)83[601:HCAIRT]2.0.CO;2.

Jackson, E. D., H. R. Shaw, and K. E. Bargar (1975), Calculated geochronology and stress field orientations along Hawaiian Chain, *Earth Planet. Sci. Lett.*, 26(2), 145–155, doi:10.1016/0012-821X(75)90082-5.

Jackson, M. G., S. R. Hart, A. A. P. Koppers, H. Staudigel, J. Konter, J. Blusztajn, M. D. Kurz, and J. A. Russell (2007a), The return of subducted continental crust in Samoan lavas, *Nature*, 448, 684–687, doi:10.1038/nature06048.

Jackson, M. G., M. D. Kurz, S. R. Hart, and R. K. Workman (2007b), New Samoan lavas from Ofu Island reveal a hemispherically heterogeneous high ^{3}He/^{4}He mantle, *Earth Planet. Sci. Lett.*, 264(3–4), 360–374, doi:10.1016/j.epsl.2007.09.023.

Jackson, M. G., S. R. Hart, J. G. Konter, A. A. P. Koppers, H. Staudigel, M. D. Kurz, J. Blusztajn, and J. M. Sinton (2010), The Samoan hotspot track on a "hotspot highway": Implications for mantle plumes and a deep Samoan mantle source, *Geochem. Geophys. Geosyst.*, 11, Q12009, doi:10.1029/2010GC003232.

Kaneoka, I. (1972), The effect of hydration on the K/Ar ages of volcanic rocks, *Earth Planet. Sci. Lett.*, 14, 216–220, doi:10.1016/0012-821X(72)90009-X.

Kear, D., and B. L. Wood (1959), *The Geology and Hydrology of Western Samoa*, Bull. N. Z. Geol. Surv., 63.

Konter, J. G., H. Staudigel, S. R. Hart, and P. M. Shearer (2004), Seafloor seismic monitoring of an active submarine volcano: Local seismicity at Vailulu'u Seamount, Samoa, *Geochem. Geophys. Geosyst.*, 5, Q06007, doi:10.1029/2004GC000702.

Konter, J. G., M. Jackson, and L. Storm (2010), Exceptional volumes of rejuvenated volcanism in Samoa, Abstract U51A-0017 presented at 2010 Fall Meeting, AGU, San Francisco, Calif., 13–17 Dec.

Koppers, A. A. P. (2002), ArArCALC—Software for ^{40}Ar/^{39}Ar age calculations, *Comput. Geosci.*, 28(5), 605–619, doi:10.1016/S0098-3004(01)00095-4.

Koppers, A. A. P., and H. Staudigel (2005), Asynchronous bends in Pacific seamount trails: A case for extensional volcanism?, *Science*, 307, 904–907, doi:10.1126/science.1107260.

Koppers, A. A. P., H. Staudigel, and J. R. Wijbrans (2000), Dating crystalline groundmass separates of altered Cretaceous seamount basalts by the Ar-40/Ar-39 incremental heating technique, *Chem. Geol.*, 166(1–2), 139–158, doi:10.1016/S0009-2541(99)00188-6.

Koppers, A. A. P., J. P. Morgan, J. W. Morgan, and H. Staudigel (2001), Testing the fixed hotspot hypothesis using Ar-40/Ar-39 age progressions along seamount trails, *Earth Planet. Sci. Lett.*, 185(3–4), 237–252, doi:10.1016/S0012-821X(00)00387-3.

Koppers, A. A. P., H. Staudigel, and R. A. Duncan (2003), High-resolution Ar-40/Ar-39 dating of the oldest oceanic basement basalts in the western Pacific basin, *Geochem. Geophys. Geosyst.*, 4(11), 8914, doi:10.1029/2003GC000574.

Koppers, A. A. P., R. A. Duncan, and B. Steinberger (2004), Implications of a non-linear ^{40}Ar/^{39}Ar age progression along the Louisville seamount trail for models of fixed and moving hotspots, *Geochem. Geophys. Geosyst.*, 5, Q06L02, doi:10.1029/2003GC000671.

Koppers, A. A. P., H. Staudigel, J. Phipps Morgan, and R. A. Duncan (2007), Non-linear ^{40}Ar/^{39}Ar age systematics along the Gilbert Ridge and Tokelau Seamount Trail and the timing of the Hawaii-Emperor Bend, *Geochem. Geophys. Geosyst.*, 8, Q06L13, doi:10.1029/2006GC001489.

Koppers, A. A. P., J. A. Russell, M. Jackson, J. Konter, H. Staudigel, and S. R. Hart (2008), Samoa reinstated as a primary hotspot trail, *Geology*, 36(6), 435–438, doi:10.1130/G24630A.1.

Kullerud, L. (1991), On the calculation of isochrons, *Chem. Geol.*, 87, 115–124.

Lanphere, M. A., and G. B. Dalrymple (1976), Identification of excess ^{40}Ar by the ^{40}Ar/^{39}Ar spectrum technique, *Earth Planet. Sci. Lett.*, 32, 141–148, doi:10.1016/0012-821X(76)90052-2.

Lin, S. C., and P. E. van Keken (2006), Dynamics of thermochemical plumes: 2. Complexity of plume structures and its implications for mapping mantle plumes, *Geochem. Geophys. Geosyst.*, 7, Q03003, doi:10.1029/2005GC001072.

Lowman, J. P., S. D. King, and C. W. Gable (2004), Steady plumes in viscously stratified, vigorously convecting, three-dimensional numerical mantle convection models with mobile plates, *Geochem. Geophys. Geosyst.*, 5, Q01L01, doi:10.1029/2003GC000583.

Mcdougall, I. (1985), Age and evolution of the volcanos of Tutuila, American Samoa, *Pac. Sci.*, 39(4), 311–320.

McDougall, I. (2010), Age of volcanism and its migration in the Samoa Islands, *Geol. Mag.*, 147(5), 705–717, doi:10.1017/s0016756810000038.

Menard, H. W. (1986), *Islands*, W. H. Freeman, Oxford, U. K.

Min, K. W., R. Mundil, P. R. Renne, and K. R. Ludwig (2000), A test for systematic errors in Ar-40/Ar-39 geochronology through comparison with U/Pb analysis of a 1.1-Ga rhyolite, *Geochim. Cosmochim. Acta*, 64(1), 73–98, doi:10.1016/S0016-7037(99)00204-5.

Montelli, R., G. Nolet, F. A. Dahlen, G. Masters, E. R. Engdahl, and S. H. Hung (2004), Finite-frequency tomo-

graphy reveals a variety of plumes in the mantle, *Science*, *303*(5656), 338–343, doi:10.1126/science.1092485.

Morgan, W. J. (1972), Deep mantle convection plumes and plate motions, *Am. Assoc. Pet. Geol. Bull.*, *56*, 42–43.

Natland, J. H. (1980), The progression of volcanism in the Samoan linear volcanic chain, *Am. J. Sci.*, *280-A*, 709–735.

Natland, J. H., and D. L. Turner (1985), Age progression and petrological development of Samoan Shield volcanoes: Evidence from K-Ar ages, lava compositions and mineral studies, in *Geological Investigations of the Northern Melanesian Borderland*, *Earth Sci. Ser.*, vol. 3, edited by T. M. Brocker, pp. 139–172, Circum-Pac. Counc. for Energy and Miner. Resour., Houston, Tex.

Natland, J., and E. L. Winterer (2005), Fissure control on volcanic action in the Pacific, in *Plumes, Plates and Paradigms*, edited by G. R. Foulger et al., *Spec. Pap. Geol. Soc. Am.*, *388*, 687–710.

Nauert, J. L., and P. B. Gans (1994), ^{40}Ar/^{39}Ar geochronology of whole-rock basalts, *U.S. Geol. Surv. Circ.*, *1107*, 231.

Németh, K., and S. J. Cronin (2009), Volcanic structures and oral traditions of volcanism of Western Samoa (SW Pacific) and their implications for hazard education, *J. Volcanol. Geotherm. Res.*, *186*(3–4), 223–237, doi:10.1016/j.jvolgeores.2009.06.010.

O'Connor, J. M., P. Stoffers, and J. R. Wijbrans (2001), En echelon volcanic elongate ridges connecting intraplate Foundation Chain volcanism to the Pacific-Antarctic spreading center, *Earth Planet. Sci. Lett.*, *189*(1–2), 93–102, doi:10.1016/S0012-821X(01)00348-X.

O'Connor, J. M., P. Stoffers, J. R. Wijbrans, and T. J. Worthington (2007), Migration of widespread long-lived volcanism across the Galapagos Volcanic Province: Evidence for a broad hotspot melting anomaly?, *Earth Planet. Sci. Lett.*, *263*(3–4), 339–354.

Oxburgh, E. R., and D. L. Turcotte (1974), Membrane tectonics and East African Rift, *Earth Planet. Sci. Lett.*, *22*(2), 133–140, doi:10.1016/0012-821X(74)90073-9.

Presley, T. K., J. M. Sinton, and M. Pringle (1997), Postshield volcanism and catastrophic mass wasting of the Waianae Volcano, Oahu, Hawaii, *Bull. Volcanol.*, *58*(8), 597–616, doi:10.1007/s004450050165.

Pringle, M. S. (1993), Age progressive volcanism in the Musicians Seamounts: A test of the hot spot hypothesis for the late Cretaceous Pacific, in *The Mesozoic Pacific: Geology, Tectonics, and Volcanism*, *Geophys. Monogr Ser.*, vol. 77, edited by M. S. Pringle et al., pp. 187–216, AGU, Washington, D. C.

Ren, Z. Y., S. Ingle, E. Takahashi, N. Hirano, and T. Hirata (2005), The chemical structure of the Hawaiian mantle plume, *Nature*, *436*(7052), 837–840, doi:10.1038/nature03907.

Renne, P. R., C. C. Swisher, A. L. Deino, D. B. Karner, T. L. Owens, and D. J. DePaolo (1998), Intercalibration of standards, absolute ages and uncertainties in Ar-40/Ar-39 dating, *Chem. Geol.*, *145*(1–2), 117–152, doi:10.1016/S0009-2541(97)00159-9.

Roddick, J. C. (1978), The application of isochron diagrams in ^{40}Ar^{-39}Ar dating: A discussion, *Earth Planet. Sci. Lett.*, *41*, 233–244, doi:10.1016/0012-821X(78)90014-6.

Rodgers, K. A., F. L. Sutherland, and P. W. O. Hoskin (Eds.) (2003), Basalts from Rose Atoll, American Samoa, *Rec. Aust. Mus.*, *55*, 141–152.

Ruellan, E., J. Delteil, I. Wright, and T. Matsumoto (2003), From rifting to active spreading in the Lau Basin–Havre Trough backarc system (SW Pacific): Locking/unlocking induced by seamount chain subduction, *Geochem. Geophys. Geosyst.*, *4*(5), 8909, doi:10.1029/2001GC000261.

Sandwell, D., and Y. Fialko (2004), Warping and cracking of the Pacific plate by thermal contraction, *J. Geophys. Res.*, *109*, B10411, doi:10.1029/2004JB003091.

Seidemann, D. E. (1977), Effects of submarine alteration on K-Ar dating of deep-sea igneous rocks, *Geol. Soc. Am. Bull.*, *88*(11), 1660–1666, doi:10.1130/0016-7606(1977)88<1660:EOSAOK>2.0.CO;2.

Seidemann, D. E. (1978), ^{40}Ar/^{39}Ar studies of deep-sea igneous rocks, *Geochim. Cosmochim. Acta*, *42*, 1721–1734.

Seidemann, D. E. (1988), The hydrothermal addition of excess ^{40}Ar to the lava flows from the Early Jurassic in the Hartford basin (northeastern U.S.A.): Implications for the time scale, *Chem. Geol.*, *72*, 37–45.

Sella, G. F., T. H. Dixon, and A. L. Mao (2002), REVEL: A model for Recent plate velocities from space geodesy, *J. Geophys. Res.*, *107*(B4), 2081, doi:10.1029/2000JB000033.

Sharp, W. D., and D. A. Clague (2006), 50-Ma initiation of Hawaiian-Emperor bend records major change in Pacific plate motion, *Science*, *313*(5791), 1281–1284, doi:10.1126/science.1128489.

Sharp, W. D., B. D. Turrin, P. R. Renne, and M. A. Lanphere (1996), The ^{40}Ar/^{39}Ar and K/Ar dating of lavas from the Hilo 1-km core hole, Hawaii Scientific Drilling Project, *J. Geophys. Res.*, *101*, 11,607–11,616, doi:10.1029/95JB03702.

Shaw, H. R., and E. D. Jackson (1973), Linear island chains in Pacific: Result of thermal plumes or gravitational anchors, *J. Geophys. Res.*, *78*(35), 8634–8652, doi:10.1029/JB078i035p08634.

Shaw, H. R., E. D. Jackson, and K. E. Bargar (1980), Volcanic periodicity along the Hawaiian Emperor Chain, *Am. J. Sci.*, *280*, 667–708.

Sims, K. W. W., S. R. Hart, M. K. Reagan, J. Blusztajn, H. Staudigel, R. A. Sohn, G. D. Layne, and L. A. Ball (2008), ^{238}U-^{230}Th-^{226}Ra-^{210}Pb-^{210}Po, ^{232}Th-^{228}Ra, and ^{235}U-^{231}Pa constraints on the ages and petrogenesis of Vailulu'u and Malumalu Lavas, Samoa, *Geochem. Geophys. Geosyst.*, *9*, Q04003, doi:10.1029/2007GC001651.

Sinton, J. M., K. T. M. Johnson, and R. C. Price (1985), Petrology and geochemistry of volcanic rocks from the northern Melanesian borderland, in *Geological Investigations of the Northern Melanesian Borderland*, vol. 3, pp. 35–65, edited by T. M. Brocker, Circum.-Pac. Counc. for Energy and Miner. Resour., Houston, Tex.

Smith, W. H. F., and D. T. Sandwell (1997), Global sea floor topography from satellite altimetry and ship depth soundings, *Science*, *277*, 1956–1962.

Staudigel, H., A. Zindler, S. R. Hart, T. Leslie, C. Y. Chen, and D. Clague (1984), The isotope systematics of a juvenile intraplate volcano: Pb, Nd, and Sr isotope ratios of basalts from Loihu Seamount, Hawaii, *Earth Planet. Sci. Lett.*, *69*(1), 13–29, doi:10.1016/0012-821X(84)90071-2.

Staudigel, H., K. H. Park, M. Pringle, J. L. Rubenstone, W. H. F. Smith, and A. Zindler (1991), The longevity of the South Pacific isotopic and thermal anomaly, *Earth Planet. Sci. Lett.*, *102*(1), 24–44, doi:10.1016/0012-821X(91)90015-A.

Staudigel, H., S. R. Hart, A. A. P. Koppers, C. Constable, R. Workman, M. Kurz, and E. T. Baker (2004), Hydrothermal venting at Vailulu'u Seamount: The smoking end of the Samoan chain, *Geochem. Geophys. Geosyst.*, *5*, Q02003, doi:10.1029/2003GC000626.

Staudigel, H., et al. (2006), Vailulu'u seamount, Samoa: Life and death on an active submarine volcano, *Proc. Natl. Acad. Sci. U. S. A.*, *103*(17), 6448–6453, doi:10.1073/pnas.0600830103.

Steiger, R. H., and E. Jäger (1977), Subcommission on geochronology: Convention on the use of decay constants in geo- and cosmochronology, *Earth Planet. Sci. Lett.*, *36*, 359–362, doi:10.1016/0012-821X(77)90060-7.

Steinberger, B. (2000), Plumes in a convecting mantle: Models and observations for individual hotspots, *J. Geophys. Res.*, *105*(B5), 11,127–11,152, doi:10.1029/1999JB900398.

Steinberger, B., and M. Antretter (2006), Conduit diameter and buoyant rising speed of mantle plumes: Implications for the motion of hot spots and shape of plume conduits, *Geochem. Geophys. Geosyst.*, *7*, Q11018, doi:10.1029/2006GC001409.

Steinberger, B., and C. Gaina (2007), Plate-tectonic reconstructions predict part of the Hawaiian hotspot tract to be preserved in the Bering Sea, *Geology*, *35*(5), 407–410, doi:10.1130/G23383A.1.

Steinberger, B., and R. J. O'Connell (1998), Advection of plumes in mantle flow: Implications for hotspot motion, mantle viscosity and plume distribution, *Geophys. J. Int.*, *132*(2), 412–434, doi:10.1046/j.1365-246x.1998.00447.x.

Steinberger, B., R. Sutherland, and R. J. O'Connell (2004), Prediction of Emperor-Hawaii seamount locations from a revised model of global plate motion and mantle flow, *Nature*, *430*(6996), 167–173, doi:10.1038/nature02660.

Tarduno, J. A., et al. (2003), The Emperor Seamounts: Southward motion of the Hawaiian hotspot plume in Earth's mantle, *Science*, *301*(5636), 1064–1069, doi:10.1126/science.1086442.

Tarduno, J., H.-P. Bunge, N. Sleep, and U. Hansen (2009), The bent Hawaiian-Emperor hotspot track: Inheriting the mantle wind, *Science*, *324*(5923), 50–53, doi:10.1126/science.1161256.

Taylor, J. R. (1997), *An Introduction to Error Analysis*, Univ. Sci. Books, Mill Valley, Calif.

Torsvik, T. H., R. D. Müller, R. Van Der Voo, B. Steinberger, and C. Gaina (2008), Global plate motion frames: Toward a unified model, *Rev. Geophys.*, *46*, RG3004, doi:10.1029/2007RG000227.

Turner, G., and P. H. Cadogan (1974), Possible effects of ^{39}Ar recoil in ^{40}Ar/^{39}Ar dating of lunar samples, *Proc. Lunar Sci. Conf.*, *5th*, 1601–1615.

Turner, D. L., and R. D. Jarrard (1982), K-Ar dating of the Cook-Austral Island Chain: A test of the hot-spot hypothesis, *J. Volcanol. Geotherm. Res.*, *12*, 187–220, doi:10.1016/0377-0273(82)90027-0.

Walker, D. A., and I. McDougall (1982), ^{40}Ar/^{39}Ar and K-Ar dating of altered glassy volcanic rocks: The Dabi volcanics, *Geochim. Cosmochim. Acta*, *46*(11), 2181–2190.

Walker, G. P. L., and P. R. Eyre (1995), Dike complexes in American Samoa, *J. Volcanol. Geotherm. Res.*, *69*(3–4), 241–254, doi:10.1016/0377-0273(95)00041-0.

Wessel, P., and L. Kroenke (1997), A geometric technique for relocating hotspots and refining absolute plate motions, *Nature*, *387*(6631), 365–369, doi:10.1038/387365a0.

Wessel, P., and L. W. Kroenke (2000), Ontong Java Plateau and late Neogene changes in Pacific plate motion, *J. Geophys. Res.*, *105*(B12), 28,255–28,277, doi:10.1029/2000JB900290.

Wessel, P., and L. W. Kroenke (2008), Pacific absolute plate motion since 145 Ma: An assessment of the fixed hot spot hypothesis, *J. Geophys. Res.*, *113*, B06101, doi:10.1029/2007JB005499.

Wessel, P., Y. Harada, and L. Kroenke (2006), Toward a self-consistent, high-resolution absolute plate motion model for the Pacific, *Geochem. Geophys. Geosyst.*, *7*, Q03L12, doi:10.1029/2005GC001000.

White, W. M., and A. W. Hofmann (1982), Sr and Nd isotope geochemistry of oceanic basalts and mantle evolution, *Nature*, *296*(5860), 821–825, doi:10.1038/296821a0.

Wilson, J. T. (1963), A possible origin of the Hawaiian Islands, *Can. J. Phys.*, *41*, 863–870.

Wolfe, C. J., S. C. Solomon, G. Laske, J. A. Collins, R. S. Detrick, J. A. Orcutt, D. Bercovici, and E. H. Hauri (2009), Mantle shear-wave velocity structure beneath the Hawaiian hot spot, *Science*, *326*(5958), 1388–1390, doi:10.1126/science.1180165.

Workman, R. K., S. R. Hart, M. Jackson, M. Regelous, K. A. Farley, J. Blusztajn, M. D. Kurz, and H. Staudigel (2004), Recycled metasomatized lithosphere as the origin of the Enriched Mantle II (EM2) end-member: Evidence from the Samoan Volcanic Chain, *Geochem. Geophys. Geosyst.*, *5*, Q04008, doi:10.1029/2003GC000623.

Workman, R. K., E. Hauri, S. R. Hart, J. Wang, and J. Blusztajn (2006), Volatile and trace elements in basaltic glasses from Samoa: Implications for water distribution in the mantle, *Earth Planet. Sci. Lett.*, *241*(3–4), 932–951, doi:10.1016/j.epsl.2005.10.028. [Erratum, *Earth Planet. Sci. Lett.*, *253*(1–2), 304, doi:10.1016/j.epsl.2006.10.031, 2007.]

Workman, R. K., J. M. Eiler, S. R. Hart, and M. G. Jackson (2008), Oxygen isotopes in Samoan lavas: Confirmation of continent recycling, *Geology*, *36*(7), 551–554, doi:10.1130/G24558A.1.

Wright, D. J. (1992), Convergence and strike-slip motion at the northern terminus of the Tonga Trench, Southwest Pacific, in *CRC Handbook of Geophysical Exploration at Sea*, edited by R. Geyer, pp. 35–79, CRC Press, Boca Raton, Fla.

Wright, D. J., S. H. Bloomer, C. J. MacLeod, B. Taylor, and A. M. Goodliffe (2000), Bathymetry of the Tonga Trench and forearc: A map series, *Mar. Geophys. Res.*, *21*(5), 489–512, doi:10.1023/A:1026514914220.

Wright, D. J., R. M. Haymon, S. M. White, and K. C. Macdonald (2002), Crustal fissuring on the crest of the southern East Pacific Rise at 17°15′–40′S, *J. Geophys. Res.*, *107*(B5), 2104, doi:10.1029/2001JB000544.

Wright, E., and W. M. White (1986), The origin of Samoa: New evidence from Sr, Nd, and Pb isotopes, *Earth Planet. Sci. Lett.*, *81*, 151–162, doi:10.1016/0012-821X(87)90152-X.

York, D. (1968), Least squares fitting of a straight line with correlated errors, *Earth Planet. Sci. Lett.*, *5*, 320–324, doi:10.1016/S0012-821X(68)80059-7.